ON THE ACCURACY OF FINITE-VOLUME
SCHEMES FOR FLUCTUATING
HYDRODYNAMICS

ALEKSANDAR DONEV, ERIC VANDEN-EIJNDEN,
ALEJANDRO GARCIA AND JOHN BELL

ON THE ACCURACY OF FINITE-VOLUME SCHEMES FOR FLUCTUATING HYDRODYNAMICS

ALEKSANDAR DONEV, ERIC VANDEN-EIJNDEN,
ALEJANDRO GARCIA AND JOHN BELL

This paper describes the development and analysis of finite-volume methods for the Landau–Lifshitz Navier–Stokes (LLNS) equations and related stochastic partial differential equations in fluid dynamics. The LLNS equations incorporate thermal fluctuations into macroscopic hydrodynamics by the addition of white-noise fluxes whose magnitudes are set by a fluctuation-dissipation relation. Originally derived for equilibrium fluctuations, the LLNS equations have also been shown to be accurate for nonequilibrium systems. Previous studies of numerical methods for the LLNS equations focused primarily on measuring variances and correlations computed at equilibrium and for selected nonequilibrium flows. In this paper, we introduce a more systematic approach based on studying discrete equilibrium structure factors for a broad class of explicit linear finite-volume schemes. This new approach provides a better characterization of the accuracy of a spatiotemporal discretization as a function of wavenumber and frequency, allowing us to distinguish between behavior at long wavelengths, where accuracy is a prime concern, and short wavelengths, where stability concerns are of greater importance. We use this analysis to develop a specialized third-order Runge–Kutta scheme that minimizes the temporal integration error in the discrete structure factor at long wavelengths for the one-dimensional linearized LLNS equations. Together with a novel method for discretizing the stochastic stress tensor in dimension larger than one, our improved temporal integrator yields a scheme for the three-dimensional equations that satisfies a discrete fluctuation-dissipation balance for small time steps and is also sufficiently accurate even for time steps close to the stability limit.

1. Introduction

Recently the fluid dynamics community has considered increasingly complex physical, chemical, and biological phenomena at the microscopic scale, including systems for which significant interactions occur across multiple scales. At a molecular scale, fluids are not deterministic; the state of the fluid is constantly changing and stochastic, even at thermodynamic equilibrium. As simulations of fluids push toward the microscale, these random thermal fluctuations play an increasingly important role in describing the state of the fluid, especially when investigating systems where the microscopic fluctuations drive a macroscopic phenomenon such as the evolution of instabilities, or where the thermal fluctuations drive the motion of suspended microscopic objects in complex fluids. Some examples in which spontaneous fluctuations can significantly affect the dynamics include the breakup of droplets in jets [56; 27; 42], Brownian molecular motors [4; 58; 24; 54], Rayleigh–Bénard convection (both single species [65] and mixtures [60]), Kolmogorov flows [14; 15; 52], Rayleigh–Taylor mixing [41; 40], combustion and explosive detonation [57; 49], and reaction fronts [55].

Numerical schemes based on a particle representation of a fluid (e.g., molecular dynamics, direct simulation Monte Carlo [2]) inherently include spontaneous fluctuations due to the irregular dynamics of the particles. However, by far the most common numerical schemes in computational fluid dynamics are based on solving partial differential equations. To incorporate thermal fluctuations into macroscopic hydrodynamics, Landau and Lifshitz introduced an extended form of the compressible Navier–Stokes equations obtained by adding white-noise stochastic flux terms to the standard deterministic equations. While they were originally developed for equilibrium fluctuations, specifically the Rayleigh and Brillouin spectral lines in light scattering, the validity of the Landau–Lifshitz Navier–Stokes (LLNS) equations for nonequilibrium systems has been assessed [28] and verified in molecular simulations [33; 51; 53]. The LLNS system is one of the more complex examples in a broad family of PDEs with stochastic fluxes. Many members of this family arise from the LLNS equations in a variety of approximations (e.g., stochastic heat equation) while others are stochastic variants of well known PDEs, such as the stochastic Burger's equation [12], which can be derived from the continuum limit of an asymmetric excluded random walk.

Several numerical approaches for fluctuating hydrodynamics have been proposed. The earliest work by Garcia et al. [32] developed a simple scheme for the stochastic heat equation and the linearized one-dimensional LLNS equations. Ladd et al. [45] have included stress fluctuations in (isothermal) Lattice Boltzmann methods for some time, and recently a better theoretical foundation has been established [1; 26]. Moseler and Landman [56] included the stochastic stress tensor of the

LLNS equations in the lubrication equations and obtain good agreement with their molecular dynamics simulation in modeling the breakup of nanojets. Sharma and Patankar [61] developed a fluid-structure coupling between a fluctuating incompressible solver and suspended Brownian particles. Coveney, De Fabritiis, Delgado-Buscalioni and coworkers have also used the isothermal LLNS equations in a hybrid scheme, coupling a continuum fluctuating solver to a molecular dynamics simulation of a liquid [29; 35; 23]. Atzberger et al. [7] have developed a version of the immersed boundary method that includes fluctuations in a pseudospectral method for the incompressible Navier–Stokes equations. Voulgarakis and Chu [63] developed a staggered scheme for the isothermal LLNS equations as part of a multiscale method for biological applications, and a similar staggered scheme was also described in [22].

Recently, Bell et al. [13] introduced a centered scheme for the LLNS equations based on interpolation schemes designed to preserve fluctuations combined with a third-order Runge–Kutta (RK3) temporal integrator. In that work, the principal diagnostic used for evaluation of the numerical method was the accuracy of the local (cell) variance and spatial (cell-to-cell) correlation structure for equilibrium and selected nonequilibrium scenarios (e.g., constant temperature gradient). The metric established by those types of tests is, in some sense, simultaneously too crude and too demanding. It is too crude in the sense that it provides only limited information from detailed simulations that cannot be directly linked to specific properties of the scheme. On the other hand, such criteria are too demanding in the sense that they place requirements on the discretization integrated over all wavelengths, requiring that the method perform well at high wavenumbers where a deterministic PDE solver performs poorly. Furthermore, although Bell et al. [13] demonstrate that RK3 is an effective algorithm, compared with other explicit schemes for the compressible Navier–Stokes equations, the general development of schemes for the LLNS equations has been mostly trial and error.

Here, our goal is to establish a more rational basis for the analysis and development of explicit finite-volume scheme for stochastic partial differential equations (SPDEs) with a stochastic flux. The approach is based on analysis of the structure factor (equilibrium fluctuation spectrum) of the discrete system. The structure factor is, in essence, the stationary spatiotemporal correlations of hydrodynamic fluctuations as a function of spatial wavenumber and temporal frequency; the static structure factor is the integral over frequency (i.e., the spatial spectrum). By analyzing the structure factor for a numerical scheme, we are able to develop notions of accuracy for a given discretization at long wavelengths. Furthermore, in many cases the theoretical analysis for the structure factor is tractable (with the aid of symbolic manipulators) allowing us to determine optimal coefficients for a given numerical scheme. We perform this optimization as a two-step procedure. First, a

spatial discretization is developed that satisfies a discrete form of the fluctuation-dissipation balance condition. Then, a stable temporal integrator is proposed and the covariances of the random numbers are chosen so as to maximize the order of temporal accuracy of the small-wavenumber static structure factor. We focus primarily on explicit schemes for solving the LLNS equations because even at the scales where thermal fluctuations are important, the limitation on time step imposed by stability is primarily due to the hyperbolic terms. That is, when the cell size is comparable to the length scale for molecular transport (e.g., mean free path in a dilute gas) the time step for these compressible hydrodynamic equations is limited by the acoustic CFL (Courant–Friedrichs–Lewy) condition. At even smaller length scales the viscous terms further limit the time step yet the validity of a continuum representation for the fluid starts to break down at those atomic scales.

The paper is divided into roughly two parts: The first half (Sections 2–4) defines notation, develops the formalism, and derives the expressions for analyzing a general class of linear stochastic PDEs from the LLNS family of equations. The main result in the first half, how to evaluate the structure factor for a numerical scheme, appears in Section 3B. The second half applies this analysis to systems of increasing complexity, starting with the stochastic heat equation (Section 5A), followed by the LLNS system in one dimension (Section 6) and three dimensions (Section 7). The paper closes with a summary and concluding remarks, followed by an Appendix on the semi-implicit Crank–Nicolson method.

2. Landau–Lifshitz Navier–Stokes equations

We consider the accuracy of explicit finite-volume methods for solving the Landau–Lifshitz Navier–Stokes (LLNS) system of stochastic partial differential equations (SPDEs) in d dimensions, given in conservative form by

$$\partial_t U = -\nabla \cdot [F(U) - \mathcal{Z}(U, r, t)], \tag{1}$$

where $U(r, t) = [\rho, j, e]^T$ is a vector of *conserved variables* that are a function of the spatial position r and time t. The conserved variables are the densities of mass ρ, momentum $j = \rho v$, and energy $e = \varepsilon(\rho, T) + \frac{1}{2}\rho v^2$, expressed in terms of the *primitive variables*, mass density ρ, velocity v, and temperature T; here ε is the internal energy density. The deterministic flux is taken from the traditional compressible Navier–Stokes–Fourier equations and can be split into *hyperbolic* and *diffusive fluxes*:

$$F(U) = F_H(U) + F_D(U),$$

where

$$F_H = \begin{bmatrix} \rho v \\ \rho v v^T + P I \\ (e + P)v \end{bmatrix} \quad \text{and} \quad F_D = -\begin{bmatrix} 0 \\ \sigma \\ \sigma \cdot v + \xi \end{bmatrix},$$

$P = P(\rho, T)$ is the pressure, the viscous stress tensor is

$$\boldsymbol{\sigma} = \eta \overline{\boldsymbol{\nabla}} \boldsymbol{v} = \eta \left[(\boldsymbol{\nabla} \boldsymbol{v} + \boldsymbol{\nabla} \boldsymbol{v}^T) - \frac{2 \, (\boldsymbol{\nabla} \cdot \boldsymbol{v})}{d} \boldsymbol{I} \right]$$

for $d \geq 2$ (we have assumed zero bulk viscosity) and $\boldsymbol{\sigma} = \eta v_x$ for $d = 1$, and the heat flux is $\boldsymbol{\xi} = \mu \boldsymbol{\nabla} T$. We denote the adjoint (conjugate transpose) of a matrix or linear operator $\boldsymbol{M}$ with $\boldsymbol{M}^{\star} = \overline{\boldsymbol{M}}^T$. As postulated by Landau and Lifshitz [46; 28], the *stochastic flux*

$$\mathcal{Z} = \begin{bmatrix} \boldsymbol{0} \\ \boldsymbol{\Sigma} \\ \boldsymbol{\Sigma} \cdot \boldsymbol{v} + \boldsymbol{\Xi} \end{bmatrix}$$

is composed of the stochastic stress tensor $\boldsymbol{\Sigma}$ and stochastic heat flux vector $\boldsymbol{\Xi}$, assumed to be mutually uncorrelated random Gaussian fields with the following covariance (where bars denote means):

$$\left\langle \boldsymbol{\Sigma}(\boldsymbol{r}, t) \boldsymbol{\Sigma}^{\star}(\boldsymbol{r}', t') \right\rangle = \boldsymbol{C}_{\boldsymbol{\Sigma}} \delta(t - t') \delta(\boldsymbol{r} - \boldsymbol{r}'),$$
$$\text{where } C^{(\boldsymbol{\Sigma})}_{ij,kl} = 2 \bar{\eta} k_B \overline{T} \big(\delta_{ik} \delta_{jl} + \delta_{il} \delta_{jk} - \tfrac{2}{d_f} \delta_{ij} \delta_{kl} \big); \quad (2)$$

$$\left\langle \boldsymbol{\Xi}(\boldsymbol{r}, t) \boldsymbol{\Xi}^{\star}(\boldsymbol{r}', t') \right\rangle = \boldsymbol{C}_{\boldsymbol{\Xi}} \delta(t - t') \delta(\boldsymbol{r} - \boldsymbol{r}'), \quad \text{where } C^{(\boldsymbol{\Xi})}_{i,j} = 2 \bar{\mu} k_B \overline{T}^2 \delta_{ij}.$$

In the LLNS system, the *hyperbolic* or *advective* fluxes are responsible for transporting the conserved quantities at the speed of sound or fluid velocity, without dissipation. On the other hand, the *diffusive* or *dissipative* fluxes are the ones responsible for damping the thermal fluctuations generated by the *stochastic* or *fluctuating* fluxes. At equilibrium a steady state is reached in which a *fluctuation-dissipation balance* condition is satisfied.

In the original formulation, Landau and Lifshitz only considered adding stochastic fluxes to the linearized Navier–Stokes equations, which leads to a well-defined system of SPDEs whose equilibrium solutions are random Gaussian fields. Derivations of the equations of fluctuating hydrodynamics through careful asymptotic expansions of the underlying microscopic (particle) dynamics give equations for the Gaussian fluctuations around the solution to the usual deterministic Navier–Stokes equations [47], in the spirit of the Central Limit Theorem. Therefore, numerical solutions should, in principle, consist of two steps: first solving the nonlinear deterministic equations for the *mean* solution, and then solving the linearized equations for the *fluctuations* around the mean. If the fluctuations are small perturbations, it makes sense numerically to try to combine these two steps into one and simply consider nonlinear equations with added thermal fluctuations. There is also hope that this might capture effects not captured in the two-system approach, such as fluctuation-

driven transport in nonequilibrium systems [59], or the effect of fluctuations on the very long-time dynamics of the mean (e.g., shock drift [13]) and hydrodynamic instabilities [65; 56; 40].

The linearized equations of fluctuating hydrodynamics can be given a well defined interpretation with the use of generalized functions or distributions [19]. However, the nonlinear fluctuating hydrodynamic equations (1) must be treated with some care since they have not been derived from first principles [28] and are in fact mathematically ill defined due to the high irregularity of white-noise fluctuating stresses [34]. More specifically, because the solution of these equations is itself a distribution the interpretation of the nonlinear terms requires giving a precise meaning to products of distributions, which cannot be defined in general and requires introducing some sort of regularization. Although written formally as an SPDE, the LLNS equations are usually interpreted in a finite volume context, where the issues of regularity, at first sight, disappear. However, in finite volume form the level of fluctuations becomes increasingly large as the volume shrinks and the nonlinear terms diverge leading to an "ultraviolet catastrophe" of the kind familiar in other fields of physics [34; 16]. Furthermore, because the noise terms are Gaussian, it is possible for rare events to push the system to states that are not thermodynamically valid such as negative T or ρ. For that reason, we will focus on the linearized LLNS equations, which can be given a well-defined interpretation. Since the fluctuations are expected to be a small perturbation of the deterministic solution, the nonlinear equations should behave similarly to the linearized equations anyway, at least near equilibrium for sufficiently large cells.

To simplify the exposition we assume the fluid to be a monoatomic ideal gas; the generalization of the results for an arbitrary fluid is tedious but straightforward. For an ideal gas the equation of state may be written as

$$P = \rho \left(k_B T / m\right) = \rho c^2,$$

where c is the isothermal speed of sound. The internal energy density is $\varepsilon = \rho c_v T$, where c_v is the heat capacity at constant volume, which may be written as $c_v = d_f k_B / 2m$ where d_f is the number of degrees of freedom of the molecules (for monoatomic gases there are $d_f = d$ translational degrees of freedom), and $c_p = (1 + 2/d_f)c_v$ is the heat capacity at constant pressure. For analytical calculations, it is convenient to convert the LLNS system from conserved variables to primitive variables, since the primitive variables are uncorrelated at equilibrium and the equations (1) simplify considerably:

$$\begin{aligned}
D_t \rho &= -\rho \nabla \cdot \boldsymbol{v}, \\
\rho \left(D_t \boldsymbol{v}\right) &= -\nabla P + \nabla \cdot \left(\boldsymbol{\sigma} + \boldsymbol{\Sigma}\right), \\
\rho c_p \left(D_t T\right) &= D_t P + \nabla \cdot \left(\boldsymbol{\xi} + \boldsymbol{\Xi}\right) + \left(\boldsymbol{\sigma} + \boldsymbol{\Sigma}\right) : \nabla \boldsymbol{v},
\end{aligned} \tag{3}$$

where $D_t\square = \partial_t\square + \boldsymbol{v}\cdot\boldsymbol{\nabla}\,(\square)$ denotes the familiar advective derivative. Note that in the fully nonlinear numerical implementation, however, we continue to use the conserved variables to ensure that the physical conservation laws are strictly obeyed.

Linearizing (3) around a reference uniform equilibrium state $\rho = \rho_0 + \delta\rho$, $\boldsymbol{v} = \boldsymbol{v}_0 + \delta\boldsymbol{v}$, $T = T_0 + \delta T$, and dropping the deltas for notational simplicity,

$$\boldsymbol{U} = \begin{bmatrix} \delta\rho \\ \delta\boldsymbol{v} \\ \delta T \end{bmatrix} \rightarrow \begin{bmatrix} \rho \\ \boldsymbol{v} \\ T \end{bmatrix},$$

we obtain the linearized LLNS system for the equilibrium thermal fluctuations,

$$\partial_t \boldsymbol{U} = -\boldsymbol{\nabla}\cdot[\boldsymbol{FU} - \boldsymbol{\mathcal{Z}}] = -\boldsymbol{\nabla}\cdot[\boldsymbol{F}_H\boldsymbol{U} + \boldsymbol{F}_D\boldsymbol{\nabla U} - \boldsymbol{\mathcal{Z}}], \tag{4}$$

where

$$\boldsymbol{F}_H\boldsymbol{U} = \begin{bmatrix} \rho_0\boldsymbol{v} + \rho\boldsymbol{v}_0 \\ (c_0^2\rho_0^{-1}\rho + c_0^2 T_0^{-1}T)\boldsymbol{I} + \boldsymbol{v}_0\boldsymbol{v}^T \\ c_0^2 c_v^{-1}\boldsymbol{v} + T\boldsymbol{v}_0 \end{bmatrix} \quad \text{and} \quad \boldsymbol{F}_D\boldsymbol{\nabla U} = \begin{bmatrix} 0 \\ \rho_0^{-1}\eta_0\overline{\boldsymbol{\nabla}}\boldsymbol{v} \\ \rho_0^{-1}c_v^{-1}\mu_0\boldsymbol{\nabla}T \end{bmatrix},$$

and $\boldsymbol{\mathcal{Z}}(\boldsymbol{r}, t)$ is a random Gaussian field with a covariance

$$\big\langle \boldsymbol{\mathcal{Z}}(\boldsymbol{r}, t)\boldsymbol{\mathcal{Z}}^\star(\boldsymbol{r}', t') \big\rangle = \boldsymbol{C}_{\boldsymbol{Z}}\delta(t - t')\delta(\boldsymbol{r} - \boldsymbol{r}'),$$

where the covariance matrix is block diagonal,

$$\boldsymbol{C}_{\boldsymbol{Z}} = \begin{bmatrix} 0 & \boldsymbol{0} & \boldsymbol{0} \\ \boldsymbol{0} & \rho_0^{-2}\boldsymbol{C}_{\boldsymbol{\Sigma}} & \boldsymbol{0} \\ \boldsymbol{0} & \boldsymbol{0} & \rho_0^{-2}c_v^{-2}\boldsymbol{C}_{\boldsymbol{\Xi}} \end{bmatrix},$$

and $\boldsymbol{C}_{\boldsymbol{\Sigma}}$ and $\boldsymbol{C}_{\boldsymbol{\Xi}}$ are given in (2). Equation (4) is a system of linear SPDEs with additive noise that can be analyzed within a general framework, as we develop next. We note that the stochastic "forcing" in (4) is essentially a divergence of white noise, modeling conservative *intrinsic* (thermal) fluctuations [47], rather than the more common *external* fluctuations modeled through white noise forcing [21; 39].

The next two sections develop the tools for analyzing finite volume schemes for linearized SPDEs, such as the LLNS system, specifically how to predict the equilibrium spectrum of the fluctuations (i.e., structure factor) from the spatial and temporal discretization used by the numerical algorithm. These analysis tools are demonstrated for simple examples in Section 5A and applied to the LLNS system in Sections 6 and 7.

3. Explicit methods for linear stochastic partial differential equations

In this section, we develop an approach for analyzing the behavior of explicit discretizations for a broad class of SPDEs, motivated by the linearized form of the LLNS equations. In particular, we consider a general linear SPDE for the stochastic field $\mathcal{U}(r, t) \equiv \mathcal{U}(t)$ of the form

$$d\mathcal{U}(t) = \mathcal{L}\mathcal{U}(t)\, dt + \mathcal{K}\, d\mathcal{B}(t), \tag{5}$$

with periodic boundary conditions on the torus $r \in \mathcal{V} = [0, H]^d$, where $\mathcal{L}$ (the *generator*) and $\mathcal{K}$ (the *filter*) are time-independent linear operators, and $\mathcal{B}$ is a cylindrical Wiener process (Brownian sheet), and the initial condition at $t = 0$ is $\mathcal{U}_0$. As common in the physics literature, we will abuse notation and write

$$\partial_t \mathcal{U} = \mathcal{L}\mathcal{U} + \mathcal{K}\mathcal{W},$$

where $\mathcal{W} = d\mathcal{B}(t)/dt$ is spatiotemporal white noise, that is, a random Gaussian field with zero mean and covariance

$$\left\langle \mathcal{W}(r, t)\mathcal{W}^\star(r', t') \right\rangle = \delta(t - t')\delta(r - r'). \tag{6}$$

The so-called mild solution [19] of (5) is a generalized process

$$\mathcal{U}(t) = e^{t\mathcal{L}}\mathcal{U}_0 + \int_0^t e^{(t-s)\mathcal{L}}\mathcal{K}\, d\mathcal{B}(s), \tag{7}$$

where the integral denotes a stochastic convolution. If the operator $\mathcal{L}$ is dissipative, that is, $\lim_{t \to \infty} e^{t\mathcal{L}}\mathcal{U}_0 = 0$ for all $\mathcal{U}_0$, then at long times t' the solution to (5) is a Gaussian process with mean zero and covariance

$$C_{\mathcal{U}}(t) = \left\langle \mathcal{U}(t')\mathcal{U}^\star(t' + t) \right\rangle = \int_{-\infty}^0 e^{-s\mathcal{L}}\mathcal{K}\mathcal{K}^\star e^{(t-s)\mathcal{L}^\star}ds, \quad t \geq 0. \tag{8}$$

This means that (5) has a unique invariant measure (equilibrium or stationary distribution) that is Gaussian with mean zero and covariance given in (8).

In general, the field $\mathcal{U}(r, t)$ is only a generalized function of the spatial coordinate r and cannot be evaluated pointwise. For the cases we will consider here, specifically, translationally invariant problems where $\mathcal{L}$ and $\mathcal{K}$ are differential operators, this difficulty can be avoided by transforming (5) to Fourier space via the Fourier series transform

$$\mathcal{U}(r, t) = \sum_{k \in \widehat{\mathcal{V}}} e^{ik \cdot r}\widehat{\mathcal{U}}(k, t), \tag{9}$$

$$\widehat{\mathcal{U}}(k, t) = \frac{1}{V}\int_{r \in \mathcal{V}} e^{-ik \cdot r}\mathcal{U}(r, t)dr, \tag{10}$$

where $V = |\mathcal{V}| = H^d$ is the volume of the system, and each *wavevector* $\boldsymbol{k} \equiv \boldsymbol{k}(\kappa)$ is expressed in terms of the integer *wave index* $\kappa \in \mathbb{Z}^d$, giving the set of discrete wavevectors

$$\widehat{\mathcal{V}} = \left\{ \boldsymbol{k} = 2\pi\kappa/H \mid \kappa \in \mathbb{Z}^d \right\}.$$

In Fourier space, the SPDE (5) becomes an infinite system of uncoupled stochastic ordinary differential equations (SODEs),

$$d\widehat{\mathcal{U}}(t) = \widehat{\mathcal{L}}\widehat{\mathcal{U}}(t)dt + \widehat{\mathcal{K}}d\widehat{\boldsymbol{\mathcal{B}}}(t), \tag{11}$$

one SODE for each $\boldsymbol{k} \in \widehat{\mathcal{V}}$. The invariant distribution of (11) is a zero-mean Gaussian random process, characterized fully by the covariance obtained from the spatial Fourier transform of (8),

$$\boldsymbol{\mathcal{S}}(\boldsymbol{k}, t) = V \left\langle \widehat{\mathcal{U}}(\boldsymbol{k}, t')\widehat{\mathcal{U}}^{\star}(\boldsymbol{k}, t' + t) \right\rangle = \frac{1}{2\pi} \int_{-\infty}^{\infty} e^{i\omega t} \boldsymbol{\mathcal{S}}(\boldsymbol{k}, \omega)d\omega, \tag{12}$$

where the *dynamic structure factor* (space-time spectrum) is

$$\boldsymbol{\mathcal{S}}(\boldsymbol{k}, \omega) = V \left\langle \widehat{\mathcal{U}}(\boldsymbol{k}, \omega)\widehat{\mathcal{U}}^{\star}(\boldsymbol{k}, \omega) \right\rangle = (\widehat{\mathcal{L}} - i\omega)^{-1}(\widehat{\mathcal{K}}\widehat{\mathcal{K}}^{\star})(\widehat{\mathcal{L}}^{\star} + i\omega)^{-1}, \tag{13}$$

which follows directly from the space-time $(\boldsymbol{k}, \omega)$ Fourier transform of the SPDE (5). By integrating the dynamic spectrum over all frequencies ω, one gets the *static structure factor*

$$\boldsymbol{\mathcal{S}}(\boldsymbol{k}) = \boldsymbol{\mathcal{S}}(\boldsymbol{k}, t = 0) = \frac{1}{2\pi} \int_{-\infty}^{\infty} \boldsymbol{\mathcal{S}}(\boldsymbol{k}, \omega)d\omega, \tag{14}$$

which is the spatial spectrum of an equilibrium snapshot of the fluctuating field and is the Fourier equivalent of $\boldsymbol{C}_{\mathcal{U}}(t = 0)$. Note that the dynamic structure factor of spatiotemporal white noise is unity independent of the wavevector and wavefrequency: $\boldsymbol{\mathcal{S}}_{\mathcal{W}}(\boldsymbol{k}, \omega) = \boldsymbol{I}$.

3A. *Discretization.* For the types of equations we will consider in this paper, the invariant measure is spatially white, specifically, $\boldsymbol{\mathcal{S}}(\boldsymbol{k})$ is diagonal and independent of $\boldsymbol{k}$. The associated fluctuating field $\mathcal{U}$ cannot be evaluated pointwise, therefore, it is more natural to use *finite-volume* cell averages, denoted here by $\boldsymbol{U}$. In the deterministic setting, for uniform periodic grids there is no important difference between finite-volume and finite-difference methods. Our general approach can likely be extended also to analysis of stochastic finite-element discretizations, however, such methods have yet to be developed for the LLNS equations and here we focus on finite-volume methods. For notational simplicity, we will discuss problems in one spatial dimension ($d = 1$), with (mostly) obvious generalizations to higher dimensions.

Space is discretized into N_c identical cells of length $\Delta x = H/N_c$, and the value U_j stored in cell $1 \leq j \leq N_c$ is the average of the corresponding variable over the cell

$$U_j(t) = \frac{1}{\Delta x} \int_{(j-1)\Delta x}^{j\Delta x} \mathcal{U}(x,t)\,dx. \qquad (15)$$

Time is discretized with a time step Δt, approximating cell averages of $\mathcal{U}(x,t)$ pointwise in time with $U^n = \{U_1^n, \ldots, U_{N_c}^n\}$,

$$U_j^n \approx U_j(n\Delta t),$$

where $n \geq 0$ enumerates the time steps. The white noise $\mathcal{W}(x,t)$ cannot be evaluated pointwise in either space or time and is discretized using a spatiotemporal average

$$\overline{\mathcal{W}}_j^n(t) = \frac{1}{\Delta x\,\Delta t} \int_{n\Delta t}^{(n+1)\Delta t} \int_{(j-1)\Delta x}^{j\Delta x} \mathcal{W}(x,t)\,dx\,dt, \qquad (16)$$

which is a normal random variable with zero mean and variance $(\Delta x\,\Delta t)^{-1}$, independent between different cells and time steps. Note that for certain types of equations the dynamic structure factor may be white in frequency as well. In this case, a pointwise-in-time discretization is not appropriate and one can instead use a spatiotemporal average as done for white noise in (16).

We will study the accuracy of explicit linear finite-volume schemes for solving the SPDE (5). Rather generally, such methods are specified by a linear recursion of the form

$$U^{n+1} = (I + L\Delta t)\,U^n + \sqrt{\frac{\Delta t}{\Delta x}}\,K W^n, \qquad (17)$$

where L and K are consistent stencil discretizations of the continuum differential operators $\mathcal{L}$ and $\mathcal{K}$ (note that L and K may involve powers of Δt in general). Here

$$W^n = (\Delta x\,\Delta t)^{1/2}\,\overline{\mathcal{W}}^n \qquad (18)$$

is a vector of standard normal variables with mean zero and variance one.

Without the random forcing, the deterministic equation $\mathcal{U}_t = \mathcal{L}\mathcal{U}$ and the associated discretization can be studied using classical tools and notions of stability, consistency, and convergence. Under the assumption that the discrete generator L is dissipative, the initial condition U^0 will be damped and the equilibrium solution will simply be a constant. The addition of the random forcing, however, leads to a nontrivial invariant measure (equilibrium distribution) of U^n determined by an interplay between the (discretized) fluctuations and dissipation. Because of the dissipative nature of the generator, any memory of the initial condition will eventually disappear and the long time dynamics is guaranteed to follow an ergodic trajectory that samples the unique invariant measure. In order to characterize

the accuracy of the stochastic integrator, we will analyze how well the discrete invariant measure (equilibrium distribution) reproduces the invariant measure of the continuum SPDE (this is a form of *weak convergence*). Note that due to ergodicity, ensemble averages can either be computed by averaging the power spectrum of the fields over multiple samples or averaging over time (after sufficiently many initial equilibration steps). In the theory we will consider the limit $n \to \infty$ and then average over different realizations of the noise W to obtain the discrete structure factors. In numerical calculations, we perform temporal averaging.

Regardless of the details of the iteration (17), W^n will always be a Gaussian random vector generated anew at each step n using a random number generator. The discretized field U^n is therefore a linear combination of Gaussian variates and it is therefore a Gaussian vector-valued stochastic process. In particular, the invariant measure (equilibrium distribution) of U^n is fully characterized by the covariance

$$C^{(U)}_{j,j',n} = \lim_{N_s \to \infty} \left\langle U_j^{N_s} \left(U_{j'}^{N_s+n} \right)^\star \right\rangle, \tag{19}$$

which we would like to compare to the covariance of the continuum Gaussian field $C_{\mathcal{U}}(t = n\Delta t)$ given by (8). This comparison is best done in the Fourier domain by using the spatial discrete Fourier transform, defined for a spatially discrete field U (for example, $U \equiv U^n$ or $U \equiv U(t)$) via

$$U_j = \sum_{k \in \widehat{\mathcal{V}}_d} \widehat{U}_k e^{ij\Delta k}, \tag{20}$$

$$\widehat{U}_k = \frac{1}{V} \sum_{j=0}^{N_c-1} U_{j+1} e^{-ij\Delta k} \Delta x, \tag{21}$$

where we have denoted the discrete *dimensionless* wavenumber

$$k\Delta x = 2\pi \kappa / N_c,$$

and the wave index is now limited to the first N_c values,

$$\widehat{\mathcal{V}}_d = \{k = 2\pi \kappa / H \mid 0 \le \kappa < N_c\} \subset \mathcal{V}.$$

Since the fields are real-valued, there is a redundancy in the Fourier coefficients $\widehat{U}_k$ because of the Hermitian symmetry between κ and $N_c - \kappa$ (essentially, the second half of the wave indices correspond to negative k), and thus we will only consider $0 \le \kappa \le \lfloor N_c/2 \rfloor$, giving a (Nyquist) cutoff wavenumber $k_{\max} \approx \pi/\Delta x$.

What we would like to compare is the Fourier coefficients of the numerical approximation, $\widehat{U}_k^n$, with the Fourier coefficients of the continuum solution

$$\widehat{\mathcal{U}}_k(t = n\Delta t).$$

The invariant measure of $\widehat{U}_k^n$ has zero mean and is characterized by the covariance obtained from the spatial Fourier transform of (19),

$$S_{k,n} = V \lim_{N_s \to \infty} \left\langle \widehat{U}_k^{N_s} \left(\widehat{U}_k^{N_s+n} \right)^\star \right\rangle. \tag{22}$$

From the definition of the discrete Fourier transform it follows that for small Δk, that is, smooth Fourier basis functions on the scale of the discrete grid, $\widehat{U}_k(t)$ converges to the Fourier coefficient $\widehat{\mathcal{U}}(k, t = n\Delta t)$ of the continuum field. Therefore, $S_{k,n}$ is the discrete equivalent (numerical approximation) to the continuum structure factor $\mathcal{S}(k, t = n\Delta t)$. We define a discrete approximation to be *weakly consistent* if

$$\lim_{\Delta x, \Delta t \to 0} S_{k,n=\lfloor t/\Delta t \rfloor} = \mathcal{S}(k, t),$$

for any chosen $k \in \widehat{\mathcal{V}}$ and t. This means that, given a sufficiently fine discretization, the numerical scheme can accurately reproduce the structure factor for a desired wave index and time lag. An alternative view is that a convergent scheme reproduces the slow (compared to Δt) and large-scale (compared to Δx) fluctuations, that is, it accurately reproduces the dynamic structure factor $\mathcal{S}(k, \omega)$ for small $\Delta k = k \Delta x$ and $\Delta \omega = \omega \Delta t$. Our goal here is to quantify this for several numerical methods for solving stochastic conservation laws and optimize the numerical schemes by tuning parameters to obtain the best possible approximation to $\mathcal{S}(k, \omega)$ for small k and ω.

Much of our analysis will be focused on the *discrete static structure factor*

$$S_k = S_{k,0} = V \lim_{N_s \to \infty} \left\langle \widehat{U}_k^{N_s} \left(\widehat{U}_k^{N_s} \right)^\star \right\rangle.$$

Note that for a spatially white field $\mathcal{U}(x)$, the finite-volume averages U_j are independent Gaussian variates with mean zero and variance Δx^{-1}, and the discrete Fourier coefficients $\widehat{U}_k$ are independent Gaussian variates with mean zero and variance V^{-1}. As a measure of the accuracy of numerical schemes for solving (5), we will compare the discrete static structure factors S_k with the continuum prediction $\mathcal{S}(k)$, for all of the discrete wavenumbers (i.e., pointwise in Fourier space). It is expected that any numerical scheme will produce some artifacts at the largest wavenumbers because of the strong corrections due to the discretization; however, small wavenumbers ought to have much smaller errors because they evolve over time scales and length scales much larger than the discretization step sizes. Specifically, we propose to look at the series expansions

$$S_k - \mathcal{S}(k) = O(\Delta t^{p_1} k^{p_2}),$$

and optimize the numerical schemes by maximizing the powers p_1 and p_2. Next we describe the general formalism used to obtain explicit expressions for the discrete structure factors S_k for a general explicit method, and then illustrate the

formalism on some simple examples, before attacking the more complex equations of fluctuating hydrodynamics.

3B. *Analysis of linear explicit methods.* Regardless of the details of a particular scheme and the particular linear SPDE being solved, at the end of the time step a typical explicit scheme makes a linear combination of the values in the neighboring cells and random variates to produce an updated value,

$$U_j^{n+1} = U_j^n + \sum_{\Delta j=-w_D}^{\Delta j=w_D} \mathbf{\Phi}_{\Delta j} U_{j+\Delta j}^n + \sum_{\Delta j=-w_S}^{\Delta j=w_S} \mathbf{\Psi}_{\Delta j} W_{j+\Delta j}^n, \tag{23}$$

where w_D and w_S are the deterministic and stochastic stencil widths. The particular forms of the matrices of coefficients $\mathbf{\Phi}$ and $\mathbf{\Psi}$ depend on the scheme, and will involve powers of Δt and Δx. Here we assume that for each n the random increment W^n is an independent vector of N_s normal variates with covariance

$$C_W = \left\langle W_j^n (W_j^n)^\star \right\rangle$$

constant for all of the cells j and thus wavenumbers, where N_s is the total number of random numbers utilized per cell per stage. Computer algebra systems can be used to obtain explicit formulas for the matrices in (23); we have made extensive use of Maple for the calculations presented in this paper.

Assuming a translation invariant scheme, the iteration (23) can easily be converted from real space to an iteration in Fourier space,

$$\widehat{U}_k^{n+1} = \widehat{U}_k^n + \sum_{\Delta j=-w_D}^{\Delta j=w_D} \mathbf{\Phi}_{\Delta j} \widehat{U}_k^n \exp(i\Delta j \Delta k) + \sum_{\Delta j=-w_S}^{\Delta j=w_S} \mathbf{\Psi}_{\Delta j} \widehat{W}_k^n \exp(i\Delta j \Delta k), \quad (24)$$

where different wavenumbers are not coupled to each other. In general, any linear explicit method can be represented in Fourier space as a recursion of the form

$$\widehat{U}_k^{n+1} = M_k \widehat{U}_k^n + N_k \widehat{W}_k^n, \tag{25}$$

where the explicit form of the matrices M_k and N_k depend on the particular scheme and typically contain various powers of $\sin \Delta k$, $\cos \Delta k$, and Δt, and

$$C_{\widehat{W}} = \left\langle \widehat{W}_k^n (\widehat{W}_k^n)^\star \right\rangle = N_c^{-1} C_W.$$

By iterating this recurrence relation, we can easily obtain (assuming $\widehat{U}_k^0 = 0$)

$$\widehat{U}_k^{n+1} = \sum_{l=0}^{n} (M_k)^l N_k \widehat{W}_k^{n-l},$$

from which we can calculate

$$S_k^n = V \left\langle \left(\widehat{U}_k^n\right)\left(\widehat{U}_k^n\right)^\star \right\rangle = \sum_{l=0}^{n-1} (M_k)^l (\Delta x N_k C_W N_k^\star)(M_k^\star)^l = \sum_{l=0}^{n-1} (M_k)^l \widetilde{C}(M_k^\star)^l.$$

In order to calculate this sum explicitly, we will use the identity

$$M_k S_k^n M_k^\star - S_k^n = (M_k)^n \widetilde{C}(M_k^\star)^n - \widetilde{C} \tag{26}$$

to obtain a linear system for the entries of the matrix S_k^n. If the deterministic method is stable, which means that all eigenvalues of the matrix M_k are below unity for all wavenumbers, then in the limit $n \to \infty$ the first term on the right side will vanish, to give

$$M_k S_k M_k^\star - S_k = -\Delta x N_k C_W N_k^\star. \tag{27}$$

If one assumes existence of a unique structure factor, Equation (27) can be most directly obtained from the condition of stationarity $S_k^{n+1} = S_k^n \equiv S_k$,

$$\left\langle \left(M_k \widehat{U}_k^n + N_k \widehat{W}_k^n\right)\left(M_k \widehat{U}_k^n + N_k \widehat{W}_k^n\right)^\star \right\rangle = \left\langle \left(\widehat{U}_k^n\right)\left(\widehat{U}_k^n\right)^\star \right\rangle = V^{-1} S_k,$$

giving a path to easily extend the analysis to more complicated situations such as multistep schemes.

Equation (27) is a linear system of equations for the equilibrium static structure factor produced by a given scheme, where the number of unknowns is equal to the square of the number of variables (field components). By simply deleting the subscripts k one obtains a more general but much larger linear system [36] for the real space equilibrium covariance of a snapshot of the discrete field $C_{j,j'}^{(U)} = C_{j,j',n=0}^{(U)}$:

$$M C_U M^\star - C_U = -\Delta x N C_W^{(N_c)} N^\star,$$

where

$$C_W^{(N_c)} = \left\langle W^n (W^n)^\star \right\rangle$$

is the covariance matrix of the random increments. Note that this relation continues to hold even for schemes that are not translation invariant such as generalizations to nonperiodic boundary conditions; however, the number of unknowns is now the square of the total number of degrees of freedom so that explicit solutions will in general not be possible. Based on standard wisdom for deterministic schemes, it is expected that schemes that perform well under periodic boundary conditions will also perform well in the presence of boundaries when the discretization is suitably modified only near the boundaries.

A similar approach to the one illustrated above for the static structure factor can be used to evaluate the discrete *dynamic* structure factor

$$S_{k,\omega} = \lim_{N_s \to \infty} V (N_s \Delta t) \left\langle \widehat{U}_{k,\omega}^{N_s} \left(\widehat{U}_{k,\omega}^{N_s}\right)^\star \right\rangle$$

from the time-discrete Fourier transform

$$\widehat{U}_{k,\omega}^{N_s} = \frac{1}{N_s} \sum_{l=0}^{N_s} \exp\left(-il\Delta\omega\right) \widehat{U}_k^l,$$

where $\Delta\omega = \omega\Delta t$, and the frequency is less than the Nyquist cutoff $\omega \leq \pi/\Delta t$. The calculation yields

$$S_{k,\omega} = [I - \exp\left(-i\Delta\omega\right) M_k]^{-1} (\Delta x \Delta t N_k C_W N_k^\star)[I - \exp\left(i\Delta\omega\right) M_k^\star]^{-1}. \quad (28)$$

Equation (28) can be seen as discretized forms of the continuum version (13) in the limits $\Delta k \to 0$, $\Delta t \to 0$ (the corresponding correlations in the time-domain are given in [36]).

Equations (27) and (28) are the main result of this section and we have used it to obtain explicit expressions for S_k and $S_{k,\omega}$ for several equations and schemes. Many of our results are in fact rather general; however, for clarity and specificity, in the next sections we will illustrate the above formalism for several simple examples of stochastic conservation laws.

3B1. *Discrete fluctuation-dissipation balance.* We consider first the static structure factors for very small time steps. In the limit $\Delta t \to 0$, temporal terms of order two or more can be ignored so that all time-integration methods behave like an explicit first-order Euler iteration as in (17),

$$\widehat{U}_k^{n+1} = \left(I + \Delta t \widehat{L}_k^{(0)}\right)\widehat{U}_k^n + \sqrt{\frac{\Delta t}{\Delta x}} \widehat{K}_k^{(0)} \widehat{W}_k, \quad (29)$$

where $L^{(0)} = L\left(\Delta t = 0\right)$ can be thought of as the spatial discretization of the generator $\mathcal{L}$, and $K^{(0)} = K\left(\Delta t = 0\right)$ is the spatial discretization of the filtering operator $\mathcal{K}$. Comparing to (25) we can directly identify $M_k = I + \Delta t \widehat{L}_k^{(0)}$ and $N_k = \sqrt{\Delta t/\Delta x}\,\widehat{K}_k^{(0)}$ and substitute these into (27). Keeping only terms of order Δt on both sides we obtain the condition

$$\widehat{L}_k^{(0)} S_k^{(0)} + S_k^{(0)} \left(\widehat{L}_k^{(0)}\right)^\star = -\widehat{K}_k^{(0)} C_W \left(\widehat{K}_k^{(0)}\right)^\star, \quad (30)$$

where $S_k^{(0)} = \lim_{\Delta t \to 0} S_k$ (see also a related real-space derivation using Ito's calculus in [6], as well as in [36, Section VIII]). It can be shown that if $\widehat{L}_k^{(0)}$ is definite, (30) has a unique solution. Assuming that W is as given in (18), that is, that $C_W = I$, and that the spatial discretizations of the generator and filter operators satisfy a *discrete fluctuation-dissipation balance*

$$\widehat{L}_k^{(0)} + \left(\widehat{L}_k^{(0)}\right)^\star = -\widehat{K}_k^{(0)} \left(\widehat{K}_k^{(0)}\right)^\star, \quad (31)$$

we see that $S_k^{(0)} = I$ is the solution to (30), that is, at equilibrium the discrete fields are spatially white. The discrete fluctuation-dissipation balance condition can also

be written in real space:

$$\boldsymbol{L}^{(0)} + (\boldsymbol{L}^{(0)})^{\star} = -\boldsymbol{K}^{(0)}(\boldsymbol{K}^{(0)})^{\star}. \tag{32}$$

The condition (32) is the discrete equivalent of the continuum fluctuation-dissipation balance condition [44]

$$\mathcal{L} + \mathcal{L}^{\star} = -\mathcal{K}\mathcal{K}^{\star}, \tag{33}$$

which ensures that $\boldsymbol{\mathcal{S}}(k) = \boldsymbol{I}$, that is, that the invariant measure of the SPDE is spatially white. We observe that adding a skew adjoint component to $\mathcal{L}$ does not alter the fluctuation-dissipation balance above, as is the case with nondissipative (advective) terms. Numerous equations [47] modeling conservative thermal systems satisfy condition (33), including the linearized LLNS equations (with some additional prefactors). In essence, the fluctuations injected at all scales by the spatially white forcing $\mathcal{W}$ are filtered by $\mathcal{K}$ and then dissipated by $\mathcal{L}$ at just equal rates.

Assuming a spatial discretization satisfies the discrete fluctuation-dissipation balance condition, it is possible to extend the above analysis to higher powers of Δt and analyze the corrections to the structure factors for finite time steps. Some general conclusions can be reached in this way, for example, the Euler method is first-order accurate, predictor-corrector methods are at least second-order accurate, while the Crank–Nicolson semi-implicit method gives $\boldsymbol{S}_k = \boldsymbol{I}$ for any time step. We will demonstrate these results for specific examples in the next section, including the spatial truncation errors as well.

4. Linear stochastic conservation laws

The remainder of this paper is devoted to the study of the accuracy of finite-volume methods for solving linear stochastic PDEs in conservation form,

$$\partial_t \mathcal{U} = -\nabla \cdot [(\boldsymbol{A}\mathcal{U} - \boldsymbol{C}\nabla\mathcal{U}) - \boldsymbol{E}\mathcal{W}], \tag{34}$$

where $\boldsymbol{A}$, $\boldsymbol{C}$ and $\boldsymbol{E}$ are constants, and $\mathcal{W}$ is Gaussian spatiotemporal white noise. The white noise forcing and its divergence here need to be interpreted in the (weak) sense of distributions since they lack the regularity required for the classical definitions. The linearization of the LLNS equations (1) leads to a system of the form (34), as do a number of other classical PDEs [47], such as the *stochastic advection-diffusion equation*

$$\partial_t T = -\boldsymbol{a} \cdot \nabla T + \mu\nabla^2 T + \sqrt{2\mu}\nabla \cdot \mathcal{W}, \tag{35}$$

where $T(\boldsymbol{r}, t) \equiv \boldsymbol{U}(\boldsymbol{r}, t)$ is a scalar stochastic field, $\boldsymbol{A} \equiv \boldsymbol{a}$ is the advective velocity, $\boldsymbol{C} \equiv \mu\boldsymbol{I}$, $\mu > 0$ is the diffusion coefficient, and $\boldsymbol{E} \equiv \sqrt{2\mu}\boldsymbol{I}$. The simplest case is the *stochastic heat equation*, obtained by taking $\boldsymbol{a} = \boldsymbol{0}$.

A key feature of the type of system considered here is that the noise is intrinsic to the system and appears in the flux as opposed to commonly treated systems that include an external stochastic forcing term, such as the form of a stochastic heat equation considered in [21]. Since white noise is more regular than the spatial derivative of white noise, external noise leads to more regular equilibrium fields (e.g., continuous functions in one dimension). Intrinsic noise, on the other hand, leads to very irregular equilibrium fields. Notationally, it is convenient to write (34) as

$$\partial_t \mathcal{U} = -\mathcal{D}(A\mathcal{U} - C\mathcal{G}\mathcal{U} - E\mathcal{W}), \tag{36}$$

defining the divergence $\mathcal{D} \equiv \nabla\cdot$ and gradient $\mathcal{G} \equiv \nabla$ operators, $\mathcal{D}^\star = -\mathcal{G}$. In the types of equations that appear in hydrodynamics, such as the LLNS equations, the operator $\mathcal{D}A$ is skew-adjoint, $(\mathcal{D}A)^\star = -\mathcal{D}A$ (hyperbolic or advective flux), $C \succeq 0$ (dissipative or diffusive flux), and $EE^\star = 2C$, that is, $E^\star = (2C)^{1/2}$. Therefore, the generator $\mathcal{L} = -\mathcal{D}A + \mathcal{D}C\mathcal{G} = (\mathcal{D}A)^\star - \mathcal{D}C\mathcal{D}^*$ and filter $\mathcal{K} = \mathcal{D}E$ satisfy the fluctuation-dissipation balance condition (33) and the equilibrium distribution is spatially white. Note that even though advection makes some of the eigenvalues of $\mathcal{L}$ complex, the generator is dissipative and (34) has a unique invariant measure because the real part of all of the eigenvalues of $\mathcal{L}$ is negative except for the unique zero eigenvalue.

It is important to point out that discretizations of the continuum operators do not necessarily satisfy the discrete fluctuation-dissipation condition (32). One way to ensure the condition is satisfied is to discretize the diffusive components of the generator $L_D = DCG$ and the filter $K = DE$ using a discrete divergence D and discrete gradient G so that the discrete fluctuation-dissipation balance condition $L_D + L_D^\star = -KK^\star$ holds. If, however, the discretization of the advective component of the generator $L_A = -DA$ is not skew-adjoint, this can perturb the balance (31). Notably, various upwinding methods lead to discretizations that are not skew-adjoint. The correction to the structure factor $S_k^{(0)} = I + \Delta S_k^{(0)}$ due to a nonzero $\Delta L_A = (L_A + L_A^\star)/2$ can easily be obtained from (30), and in one dimension the result is simply

$$\Delta S_k^{(0)} = -\frac{\Delta L_k^{(A)}}{L_k^{(D)} + \Delta L_k^{(A)}}. \tag{37}$$

We will use centered differences for the advective generator in this work, which ensures a skew-adjoint L_A, and our focus will therefore be on satisfying the discrete fluctuation-dissipation balance between the diffusive and stochastic terms.

4A. *Finite-volume numerical schemes.* We consider here rather general finite-volume methods for solving the linear SPDE (34) in one dimension,

$$\partial_t \mathcal{U} = -\frac{\partial}{\partial x}[\mathcal{F}(\mathcal{U}) - \mathcal{Z}] = -\frac{\partial}{\partial x}\left[\left(A - C\frac{\partial}{\partial x}\right)\mathcal{U} - E\mathcal{W}\right] \tag{38}$$

with periodic boundaries, where we have denoted the stochastic flux with $\mathcal{Z} = E\mathcal{W}$. As for classical finite-volume methods for the deterministic case, we start from the PDE and integrate the left and right sides over a given cell j over a given time step Δt, and use integration by parts to obtain the formally exact

$$U_j^{n+1} = U_j^n - \frac{\Delta t}{\Delta x}(F_{j+1/2} - F_{j-1/2}) + \frac{\Delta t}{\Delta x}\left(\frac{1}{\sqrt{\Delta x \Delta t}}\right)(Z_{j+1/2} - Z_{j-1/2}), \quad (39)$$

where the *deterministic discrete fluxes* F and *stochastic discrete fluxes* Z are calculated on the boundaries of the cells (points in one dimension, edges in two dimensions, and faces in three dimensions), indexed here with half-integers. These fluxes represent the total rate of transport through the interface between two cells over a given finite time interval Δt, and (39) is nothing more than a restatement of conservation. The classical interpretation of pointwise evaluation of the fluxes is not appropriate because white noise forcing lacks the regularity of classical smooth forcing and cannot be represented in a finite basis. Instead, just as we projected the fluctuating fields using finite-volume averaging, we ought to project the stochastic fluxes $\mathcal{Z}$ to a finite representation $\overline{\mathcal{Z}} = (\Delta x \Delta t)^{-1/2} Z$ through spatio-temporal averaging, as done in (16) and (18). For the purposes of our analysis, one can simply think of the discrete fluxes as an approximation that has the same spectral properties as the corresponding continuum Gaussian fields over the wavevectors and frequencies represented by the finite discretization.

The goal of numerical methods is to approximate the fluxes as best as possible. In general, within each time step of a scheme there may be N_{st} stages or substeps; for example, in the classic MacCormack method there is a predictor and a corrector stage ($N_{st} = 2$), and in the three-stage Runge–Kutta method of Williams et al. [13], there are three stages ($N_{st} = 3$). Each stage $0 < s \le N_{st}$ is of the conservative form (39):

$$U_j^{n+s/N_{st}} = \sum_{s'=0}^{s-1} \alpha_{s'}^{(s)} U_j^{n+s'/N_{st}} - \frac{\Delta t}{\Delta x}(F_{j+1/2}^{(s)} - F_{j-1/2}^{(s)})$$
$$+ \frac{\Delta t^{1/2}}{\Delta x^{3/2}}(Z_{j+1/2}^{(s)} - Z_{j-1/2}^{(s)}), \quad (40)$$

where the α's are some coefficients, $\sum_{s'=0}^{s-1} \alpha_{s'}^{(s)} = 1$, and each of the stage fluxes are partial approximations of the continuum flux. For the stochastic integrators we discuss here, the deterministic fluxes are calculated the same way as they would be in the corresponding deterministic scheme. In general, the stochastic fluxes $Z_{j+1/2}$ can be expressed in terms of independent unit normal variates $W_{j+1/2}$ that are sampled using a random number generator. The stochastic fluxes in each stage may be the same, may be completely independent, or they may have nontrivial correlations between stages.

Note that it is possible to avoid noninteger indices by reindexing the fluxes in (39) and writing it in a form consistent with (23):

$$U_j^{n+1} = U_j^n - \frac{\Delta t}{\Delta x}(F_j - F_{j-1}) + \frac{\Delta t^{1/2}}{\Delta x^{3/2}}(Z_j - Z_{j-1}). \qquad (41)$$

However, when considering the order of accuracy of the stencils and also fluctuation-dissipation balance in higher dimensions, it will become important to keep in mind that the fluxes are evaluated on the faces (edges or half-grid points) of the grid, and therefore we will keep the half-integer indices. Note that for face-centered values, such as fluxes, it is best to add a phase factor $\exp(i\,\Delta k/2)$ in the definition of the Fourier transform, even though such pure phase shifts will not affect the correlation functions and structure factors.

Before we analyze schemes for the complex LLNS equations, we present an illustrative explicit calculation for the one-dimensional stochastic heat equation.

5. Example: stochastic heat equation

We now illustrate the general formalism presented in Section 4 for the simple case of an Euler and predictor-corrector scheme for solving the stochastic heat equation in one dimension,

$$v_t = \mu v_{xx} + \sqrt{2\mu}\mathcal{W}_x, \qquad (42)$$

where $v(x, t) \equiv \mathcal{U}(x, t)$ is a scalar field and μ is the mass or heat diffusion coefficient. The solution in the Fourier domain is trivial, giving

$$S(k, \omega) = \frac{2\mu k^2}{\omega^2 + \mu^2 k^4} \quad \text{and} \quad S(k) = 1. \qquad (43)$$

5A. *Static structure factor.* We first study a simple second-order spatial discretization of the dissipative fluxes

$$F_{j+1/2} = \frac{\mu}{\Delta x}(u_{j+1} - u_j),$$

combined with an Euler integration in time, to give a simple numerical method for solving the SPDE (42):

$$u_j^{n+1} = u_j^n + \frac{\mu\Delta t}{\Delta x^2}(u_{j-1}^n - 2u_j^n + u_{j+1}^n) + \sqrt{2\mu}\frac{\Delta t^{1/2}}{\Delta x^{3/2}}(W_{j+1/2}^n - W_{j-1/2}^n), \quad (44)$$

where $u \equiv U$ and the W's are independent unit normal random numbers with zero mean generated anew at every time step (here $N_s = N_{st} = 1$). From (44), we can extract the recursion coefficients appearing in (25),

$$M_k = 1 + \beta(e^{-i\,\Delta k} - 2 + e^{i\,\Delta k}) = 1 + 2\beta\,(\cos\Delta k - 1),$$

$$N_k = \sqrt{2\mu}\frac{\Delta t^{1/2}}{\Delta x^{3/2}}(e^{i\,\Delta k/2} - e^{-i\,\Delta k/2}),$$

where

$$\beta = \frac{\mu \Delta t}{\Delta x^2}$$

denotes a dimensionless diffusive time step (ratio of the time step to the diffusive CFL limit). Together with $C_W = 1$, Equation (27) becomes a scalar equation for the discrete structure factor

$$(M_k M_k^\star - 1)S_k = -\Delta x N_k N_k^\star,$$

with dimensionless solution

$$S_k = \frac{4\beta(1 - \cos \Delta k)}{(1 - M_k^2)} = [1 + \beta(\cos \Delta k - 1)]^{-1}. \tag{45}$$

The time-dependent result can also easily be derived from (26):

$$S_k^n = (1 - e^{-t/\tau})S_k, \quad \text{where } t = n\Delta t,$$

and $\tau^{-1} = 4\mu (\cos \Delta k - 1)/\Delta x^2 \approx 2\mu k^2$ is the familiar relaxation time for wavenumber k, showing that the smallest wavenumbers take a long time to reach the equilibrium distribution.

Equation (45) is a vivid illustration of the typical result for schemes for stochastic transport equations based on finite difference stencils, also shown in Figure 1. Firstly, we see that for small k we have that $S_k \approx 1 + \beta \Delta k^2/2$, showing that the smallest wavenumbers are correctly handled by the discretization for any time step. Also, this shows that the error in the structure factor is of order β, that is, of order Δt, as expected for the Euler scheme, whose weak order of convergence is one for SODEs. Finally, it shows that the error grows quadratically with k (from symmetry arguments, only even powers will appear). By looking at the largest wavenumber, $\Delta k_{\max} = \pi$, we see that $S_{k_{\max}} = (1 - 2\beta)^{-1}$, from which we instantly see the CFL stability condition $\beta < 1/2$, which guarantees that the structure factor is finite and positive for all $0 \le k \le \pi$. Furthermore, we see that for $\beta \ll 1$, the structure factor is approximately unity for all wavenumbers. That is, a sufficiently small step will indeed reproduce the proper equilibrium distribution.

By contrast, a two-stage predictor-corrector scheme for the diffusion equation,

$$\tilde{u}_j^n = u_j^n + \frac{\mu \Delta t}{\Delta x^2}(u_{j-1}^n - 2u_j^n + u_{j+1}^n) + \sqrt{2\mu}\frac{\Delta t^{1/2}}{\Delta x^{3/2}}(W_{j+1/2}^n - W_{j-1/2}^n),$$

$$u_j^{n+1} = \frac{1}{2}\left[u_j^n + \tilde{u}_j^n + \frac{\mu \Delta t}{\Delta x^2}(\tilde{u}_{j-1}^n - 2\tilde{u}_j^n + \tilde{u}_{j+1}^n) + \sqrt{2\mu}\frac{\Delta t^{1/2}}{\Delta x^{3/2}}(W_{j+1/2}^n - W_{j-1/2}^n)\right]. \tag{46}$$

achieves much higher accuracy, namely, a structure factor that deviates from unity by a higher order in both Δt and k,

$$\text{PC-1RNG: } S_k \approx 1 - \tfrac{1}{4}\beta^2 \Delta k^4,$$
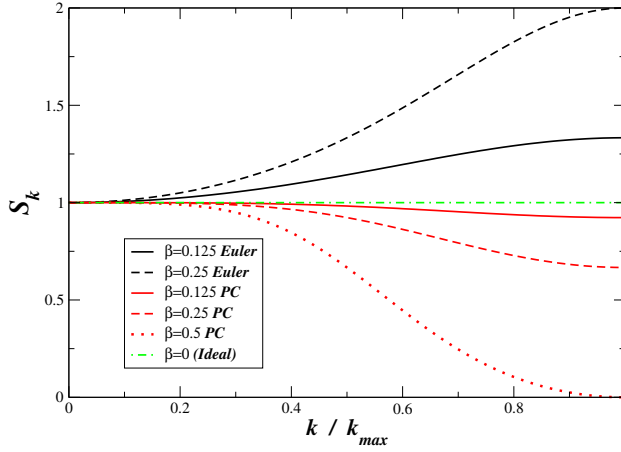
Figure 1. An illustration of the discrete structure factor S_k for the Euler (44) and predictor-corrector (46) schemes for the stochastic heat equation (42).

as illustrated in Figure 1. We can also use different stochastic fluxes in the predictor and the corrector stages (i.e., use $N_s = 2$ random numbers per cell per stage), with an added prefactor of $\sqrt{2}$ to compensate for the variance reduction of the averaging between the two stages,

$$
\begin{aligned}
\tilde{u}_j^n &= u_j^n + \frac{\mu \Delta t}{\Delta x^2}(u_{j-1}^n - 2u_j^n + u_{j+1}^n) + 2\sqrt{\mu}\frac{\Delta t^{1/2}}{\Delta x^{3/2}}\left(W_{j+1/2}^{(n,P)} - W_{j-1/2}^{(n,P)}\right), \\
u_j^{n+1} &= \frac{1}{2}\left[u_j^n + \tilde{u}_j^n + \frac{\mu \Delta t}{\Delta x^2}(\tilde{u}_{j-1}^n - 2\tilde{u}_j^n + \tilde{u}_{j+1}^n) + 2\sqrt{\mu}\frac{\Delta t^{1/2}}{\Delta x^{3/2}}(W_{j+1/2}^{(n,C)} - W_{j-1/2}^{(n,C)})\right].
\end{aligned}
\tag{47}
$$

For the scheme (47) the analysis reveals an even greater spatiotemporal accuracy of the static structure factors, namely, third order temporal accuracy:

$$
\text{PC-2RNG: } S_k \approx 1 + \tfrac{1}{8}\beta^3 \Delta k^6.
$$

This illustrates the importance of the handling of the stochastic fluxes in multi-stage algorithms, as we will come back to shortly. Note, however, that the PC-1RNG method (46) may be preferred in practice over the PC-2RNG method (47) even though using two random numbers per step gives greater accuracy for small wavenumbers for small time steps. This is not only because of the computational savings of generating half the random numbers, but also because PC-1RNG is better-behaved (more stable) at large wavenumbers for large time steps. Specifically, the structure factor can become rather large for $\Delta k = \pi$ for PC-2RNG for $\beta > 0.1$.

The analysis we presented here for explicit methods can easily be extended to implicit and semi-implicit schemes as well, as illustrated in the Appendix for the Crank–Nicolson method for the stochastic heat equation.

Previous studies [13; 29] have measured the accuracy of numerical schemes through the *variance* of the fields in real space, which, by Parseval's theorem, is related to the integral of the structure factor over all wavenumbers. For the Euler scheme (44) for the stochastic heat equation this can be calculated analytically,

$$\sigma_u^2 = \langle u_j^2 \rangle - \langle u_j \rangle^2 = \Delta x^{-1}(1-2\beta)^{-1/2} \approx \Delta x^{-1}(1+\beta),$$

showing first-order temporal accuracy (in the weak sense). For the predictor-corrector scheme (46), on the other hand,

$$(\sigma_u^{PC})^2 \approx \Delta x^{-1}(1-3\beta^2/2).$$

It is important to note, however, that using the variance as a measure of accuracy of stochastic real-space integrators is both too rough and also too stringent of a test. It does not give insights into how well the equipartition is satisfied for the different modes, and, at the same time, it requires that the structure factor be good even for the highest wavenumbers, which is unreasonable to ask from a finite-stencil scheme.

For pseudospectral methods, as studied for the incompressible fluctuating Navier–Stokes equation in [8; 43], one can modify the spectrum of the stochastic forcing so as to balance the numerical stencil artifacts, and one can also use an (exact) exponential temporal integrator in Fourier space to avoid the artifacts of time stepping. However, for finite-volume schemes, a more reasonable approach is to keep the stochastic fluxes uncorrelated between disjoint cells (which is actually physical), and instead of looking at the variance, focus on the accuracy of the static structure factor for small wavenumbers. Specifically, basic schemes will typically have $S_k - 1 = O(\Delta t k^2)$, while multistep schemes will typically achieve $S_k - 1 = O(\Delta t^2 k^2)$ or higher temporal order, or even $S_k - 1 = O(\Delta t^2 k^4)$.

5B. *Dynamic structure factor.* It is also constructive to study the full dynamic structure factor for a given numerical scheme, especially for small wavenumbers and low frequencies. This is significantly more involved in terms of analytical calculations and the results are algebraically more complicated, especially for multistage methods and more complex equations. For the Euler scheme (44) the solution to (28) is

$$S_{k,\omega} = \frac{2\chi_1 \chi_2^{-1} \mu k^2}{2\Delta t^{-2}\,(1-\cos \Delta\omega) + \chi_1^2 \chi_2^{-1}\mu^2 k^4},$$

where $\chi_1 = 2(1-\cos \Delta k)/\Delta k^2$ and $\chi_2 = 1+2\beta\,(\cos \Delta k - 1)$. This shows that the dynamic structure factor does not converge to the correct answer for all wavenumbers

even in the limit $\Delta t \to 0$, namely,

$$\lim_{\beta \to 0} S_{k,\omega} = \frac{2\chi_1 \mu k^2}{\omega^2 + \chi_1^2 \mu^2 k^4}. \tag{48}$$

For small Δk, $\chi_1 \approx 1 - \Delta k^2/6$, and the numerical result closely matches the theoretical result (43). However, for finite wavenumbers the effective diffusion coefficient is multiplied by a prefactor χ_1, which represents the spatial truncation error in the second-order approximation to the Laplacian. For all of the time-integration schemes for the stochastic heat equation discussed above, one can reduce the discrete dynamic structure factor to a form

$$S_{k,\omega} = \frac{2\chi_{\text{stoch}} \mu k^2}{2\Delta t^{-2} (1 - \cos \Delta\omega) + \chi_{\text{det}}^2 \mu^2 k^4},$$

where χ_{stoch} and χ_{det} depend on β and Δk and can be used to judge the accuracy of the scheme.

In this paper we focus on the static structure factors in order to optimize the numerical schemes and then simply check numerically that they also produce reasonably accurate results for the dynamic structure factors for small and intermediate wavenumbers and frequencies.

5C. *Higher-order differencing.* Another interesting question is whether using a higher-order differencing formula for the viscous fluxes improves upon the second-order formula in the basic Euler scheme (44). For example, a standard fourth order in space finite difference yields the modified Euler scheme

$$u_j^{n+1} = u_j^n + \frac{\mu \Delta t}{12\Delta x^2}(-u_{j-2}^n + 16u_{j-1}^n - 30u_j^n + 16u_{j+1}^n - u_{j+2}^n)$$

$$+ \sqrt{2\mu} \frac{\Delta t^{1/2}}{\Delta x^{3/2}} (W_{j+1/2} - W_{j-1/2}). \tag{49}$$

Repeating the previous calculation shows that

$$\lim_{\beta \to 0} S_k = 6 [7 - \cos \Delta k]^{-1}, \tag{50}$$

demonstrating that the fluctuation-dissipation theorem is not satisfied for this scheme at the discrete level even for infinitesimal time steps. This is because the spatial discretization operators in (49) do not satisfy the discrete fluctuation dissipation balance.

In order to obtain higher-order divergence and Laplacian stencils that satisfy (31) we can start from a higher order divergence discretization $\boldsymbol{D}$ and then simply calculate the resulting discrete Laplacian $\boldsymbol{L} = -\boldsymbol{D}\boldsymbol{D}^\star$. Here $\boldsymbol{D}$ should be a fourth-order (or higher) difference formula that combines four face-centered values, two

on each side of a given cell, into an approximation to the derivative at the cell center. Conversely, $\boldsymbol{D}^{\star}$ combines the values from four cells, two on each side of a given face, into an approximation to the derivative at the face center. A standard fourth-order finite-difference stencil for $\boldsymbol{D}$ produces the *higher-order Euler scheme*

$$u_j^{n+1} = u_j^n + \frac{\mu \Delta t}{\Delta x^2} \left(\frac{1}{576} u_{j-3}^n - \frac{3}{32} u_{j-2}^n + \frac{87}{64} u_{j-1}^n - \frac{365}{144} u_j^n + \frac{87}{64} u_{j+1}^n - \frac{3}{32} u_{j+2}^n + \frac{1}{576} u_{j+3}^n \right)$$
$$+ \sqrt{2\mu} \frac{\Delta t^{1/2}}{\Delta x^{3/2}} \left(\frac{1}{24} W_{j-3/2} - \frac{9}{8} W_{j-1/2} + \frac{9}{8} W_{j+1/2} - \frac{1}{24} W_{j+3/2} \right), \qquad (51)$$

for which $S_k \approx 1 + \beta \Delta k^2 / 2$, which is the same leading-order error as the basic Euler scheme (44). On the other hand, the dynamic structure factor for small time steps is as in (48) but now

$$\chi_1 = (1 - \cos \Delta k)(13 - \cos \Delta k) / \left(72 \Delta k^2 \right) \approx 1 - \tfrac{3}{320} \Delta k^4,$$

which shows the higher spatial order of the scheme.

Note that in (51) both the discretization of the Laplacian and of the gradient are of higher spatial order than in (44), however, the Laplacian operator is not of the highest order possible for the given stencil width. We will not use higher-order differencing for the diffusive fluxes in this work in order to avoid large Laplacian stencils like the one above. Rather, we will use the traditional second-order discretization and focus on the time integration of the resulting system.

5D. *Handling of advection.* The analysis we illustrated here for the stochastic heat equation can be directly applied to the scalar advection-diffusion equation (35) in one dimension:

$$v_t = -a v_x + \mu v_{xx} + \sqrt{2\mu} \mathcal{W}_x. \qquad (52)$$

For example, a second-order centered difference discretization of the advective term $-a v_x$ leads to the following explicit Euler scheme

$$u_j^{n+1} = u_j^n - \frac{\alpha}{2} (u_{j+1}^n - u_{j-1}^n) + \beta (u_{j-1}^n - 2u_j^n + u_{j+1}^n)$$
$$+ \sqrt{2\mu} \frac{\Delta t^{1/2}}{\Delta x^{3/2}} (W_{j+1/2}^n - W_{j-1/2}^n), \quad (53)$$

where the dimensionless advective CFL number is

$$\alpha = \frac{a \Delta t}{\Delta x} = \beta r,$$

and $r = a \Delta x / \mu$ is the so-called cell Reynolds number and measures the relative importance of advective and diffusive terms at the grid scale. Note that this scheme is unconditionally unstable when $\mu = 0$, specifically, the stability condition is $\alpha^2 / 2 \leq \beta \leq 1/2$.

For the Euler method (53) the analysis yields a structure factor

$$S_k \approx \frac{1}{1 - \alpha r/2} + \frac{(1 - r^2/4)}{2(1 - \alpha r/2)^2} \beta \Delta k^2,$$

showing that even the smallest wavenumbers have the wrong spectrum for a finite time step when $|r| > 0$, which is unacceptable in practice since it means that even the slowly evolving large-scale fluctuations are not handled correctly. Adding an artificial diffusion $\Delta \mu = \mu \, |r| \, /2$ to μ leads to an improved leading order error:

$$S_k \approx 1 + \tfrac{1}{2}(1 - r^2/4)\beta \Delta k^2 + O(\Delta t^2 \Delta k^2).$$

It is well known that adding such an artificial diffusion is equivalent to upwinding the advective term and leads to much improved stability for large r as well.[1]

The second-order predictor-corrector time stepping scheme can be applied when advection is included as well. If $|r| > 0$, the leading order errors are

$$\text{PC-1RNG: } S_k \approx 1 - \tfrac{1}{4}\alpha^2\left(1 - \tfrac{1}{2}r\alpha\right)\Delta k^2, \tag{54}$$

$$\text{PC-2RNG: } S_k \approx 1 - \tfrac{1}{8}r\alpha^3\Delta k^2, \tag{55}$$

showing that PC-2RNG gives a more accurate discrete structure factor than PC-1RNG for small wavenumbers and time steps. Note that the predictor-corrector method is unconditionally unstable when $\mu = 0$. In Section 6A we analyze a three-stage Runge–Kutta scheme that has a small leading order error in S_k but is also stable when $\alpha < 1$ even if $\mu = 0$.

6. LLNS equations in one dimension

In this section, we will consider the linearized LLNS system (4) for a monoatomic ideal gas in one spatial dimension, that is, where symmetry dictates variability along only the x axis. As explained in the Introduction, focusing on an ideal gas simply fixes the values of certain coefficients and thus simplifies the algebra, without limiting the generality of our analysis. We will arbitrarily choose the number of degrees of freedom per particle to be $d_f = 1$, even though in most cases of physical interest $d_f = 3$ is appropriate; this merely changes some of the constant coefficients and does not affect our discussion. Explicitly, the one-dimensional linearized LLNS

---

[1] Note that for this particular type of upwinding the denominator in (37) vanishes identically and it can be shown that the correct solution is $\Delta S_k^{(0)} = 0$; however, this is not necessarily true for other, higher order, upwind discretizations of advection.

equations are

$$
\begin{bmatrix} \partial_t \rho \\ \partial_t v \\ \partial_t T \end{bmatrix} = -\frac{\partial}{\partial x} \begin{bmatrix} \rho_0 v + \rho v_0 \\ c_0^2 \rho_0^{-1} \rho + c_0^2 T_0^{-1} T + v_0 v \\ c_0^2 c_v^{-1} v + T v_0 \end{bmatrix}
$$
$$
+ \frac{\partial}{\partial x} \begin{bmatrix} 0 \\ \rho_0^{-1} \eta_0 v_x \\ \rho_0^{-1} c_v^{-1} \mu_0 T_x \end{bmatrix} + \frac{\partial}{\partial x} \begin{bmatrix} 0 \\ \rho_0^{-1} \Sigma \\ \rho_0^{-1} c_v^{-1} \Xi \end{bmatrix}, \tag{56}
$$

where the covariance matrices of the stochastic fluxes are $C_\Sigma = 2\eta_0 k_B T_0$ and $C_\Xi = 2\mu_0 k_B T_0^2$. In Fourier space the flux becomes

$$
\widehat{F} = \begin{bmatrix} v_0 & \rho_0 & 0 \\ \rho_0^{-1} c_0^2 & (v_0 - ik\rho_0^{-1}\eta_0) & T_0^{-1} c_0^2 \\ 0 & c_0^2 c_v^{-1} & (v_0 - ik\rho_0^{-1}c_v^{-1}\mu_0) \end{bmatrix},
$$

which through Equations (13) and (14) (or, equivalently, (30)) gives static structure factors that are independent of k:

$$
S(k) = \begin{bmatrix} \rho_0 c_0^{-2} k_B T_0 & 0 & 0 \\ 0 & \rho_0^{-1} k_B T_0 & 0 \\ 0 & 0 & \rho_0^{-1} c_v^{-1} k_B T_0^2 \end{bmatrix}. \tag{57}
$$

Therefore, the invariant distribution for the fluctuating fields is spatially-white, with no correlations among the different primitive variables, and with variances given in (57). This is in agreement with predictions of statistical mechanics, and how Landau and Lifshitz obtained the form of the stochastic fluxes. Note that in the incompressible limit, $c_0 \to \infty$, the density fluctuations diminish, but the velocity and temperature fluctuations are independent of c_0.

In this section we will calculate the discrete structure factor for several finite-volume approximations to (56). From the diagonal elements of S_k we can directly obtain the nondimensionalized static structure factors for the three primitive variables, for example,

$$
S_k^{(\rho)} = \frac{V}{\rho_0 c_0^{-2} k_B T_0} \langle \hat{\rho}_k \hat{\rho}_k^\star \rangle,
$$

which for a perfect scheme would be unity for all wavevectors. Similarly, the off-diagonal or cross elements, such as, for example,

$$
S_k^{(\rho,v)} = \frac{V}{\sqrt{(\rho_0 c_0^{-2} k_B T_0)(\rho_0^{-1} k_B T_0)}} \langle \hat{\rho}_k \hat{v}_k^\star \rangle,
$$

would all vanish for all wavevectors for a perfect scheme. Our goal will be to quantify the deviations from "perfect" for several methods, as a function of the discretization parameters Δx and Δt.

6A. *Third-order Runge–Kutta* (**RK3**) *scheme.* When designing numerical schemes to integrate the full LLNS system, it seems most appropriate to base the scheme on well known robust deterministic methods, and modify the deterministic methods by simply adding a stochastic component to the fluxes, in addition to the usual deterministic component. With such an approach, at least we can be confident that in the case of weak noise the solver will be robust and thus we will not compromise the fluid solver just to accommodate the fluctuations.

A well known approach to solving PDEs in conservation form

$$\partial_t \mathcal{U} = -\nabla \cdot [\mathcal{F}(\mathcal{U})] = -\nabla \cdot [\mathcal{F}_H(\mathcal{U}) + \mathcal{F}_D(\nabla \mathcal{U})]$$

is to use the *method of lines* to decouple the spatial and temporal discretizations. We will focus on one dimension first for notational simplicity. In the method of lines, a finite-volume spatial discretization is applied to the obtain a system of differential equations for the discretized fields

$$\begin{aligned}
\frac{d\boldsymbol{U}_j}{dt} &= -\Delta x^{-1}[\boldsymbol{F}_{j+1/2}(\boldsymbol{U}) - \boldsymbol{F}_{j-1/2}(\boldsymbol{U})]\\
&= -\Delta x^{-1}[\boldsymbol{F}_H(\boldsymbol{U}_{j+1/2}) - \boldsymbol{F}_H(\boldsymbol{U}_{j-1/2})]\\
&\quad -\Delta x^{-1}[\boldsymbol{F}_D(\nabla_{j+1/2}\boldsymbol{U}) - \boldsymbol{F}_D(\nabla_{j-1/2}\boldsymbol{U})],
\end{aligned} \tag{58}$$

where $\boldsymbol{U}_{j+1/2}$ are face-centered values of the fields that are calculated from the cell-centered values $\boldsymbol{U}_j$, and $\nabla_{j+1/2}$ is a cell-to-face discretization of the gradient operator. Any classical temporal integrator can be applied to the resulting system of semidiscrete system. It is well known that the Euler and Heun (two-step second-order Runge–Kutta) methods are unconditionally unstable for hyperbolic equations. In [13], an algorithm for the solution of the LLNS system of equations (1) was proposed, which is based on the three-stage, low-storage TVD Runge–Kutta (RK3) scheme of Gottlieb and Shu [37]. The RK3 scheme is the simplest TVD RK discretization for the deterministic compressible Navier–Stokes equations that is stable even in the inviscid limit, with the omission of slope-limiting. Here we adopt the same basic scheme and investigate optimal ways of evaluating the stochastic flux.

In the RK3 scheme, the hyperbolic component of the face flux $\boldsymbol{F}_H$ is calculated by a cubic interpolation of $\boldsymbol{U}$ from the cell centers to the faces using an interpolation formula borrowed from PPM (piecewise parabolic method), [18],

$$\boldsymbol{U}_{j+1/2} = \tfrac{7}{12}(\boldsymbol{U}_j + \boldsymbol{U}_{j+1}) - \tfrac{1}{12}(\boldsymbol{U}_{j-1} + \boldsymbol{U}_{j+2}), \tag{59}$$

and then directly evaluating the hyperbolic flux from the interpolated values. In [13; 10] a modified interpolation is proposed that preserves variances; however, our analytical calculations indicate that this type of interpolation artificially increases the structure factor for intermediate wavenumbers in order to compensate for the errors at larger wavenumbers. Note that for the full nonlinear equations, either the conserved or the primitive quantities can be interpolated. For the linearized equations it does not matter and it is simpler to work exclusively with primitive variables.

In the RK3 method, the diffusive components of the fluxes $\boldsymbol{F}_D$ are calculated using classical face-centered second-order centered stencils to evaluate the gradients of the fields at the cell faces. Stochastic fluxes $\boldsymbol{Z}_{j+1/2}$ are also generated at the faces of the grid using a standard random number generator (RNG). These stochastic fluxes are generated independently for velocity and temperature, and are zero for density,

$$
\boldsymbol{Z}_{j+1/2}^{(RNG)} = \begin{bmatrix} 0 \\ \rho_0^{-1} (2\eta_0 k_B T_0)^{1/2} W_{j+1/2}^{(1)} \\ \rho_0^{-1} c_v^{-1} (2\mu_0 k_B T_0^2)^{1/2} W_{j+1/2}^{(2)} \end{bmatrix},
$$

where $W_{j+1/2}^{(1/2)}$ denotes a normal variate with zero mean and unit variance.

For each stage of the RK3 scheme, a total cell increment is calculated as

$$
\Delta \boldsymbol{U}_j(\boldsymbol{U}, \boldsymbol{W}) = -\frac{\Delta t}{\Delta x} [\boldsymbol{F}_{j+1/2}(\boldsymbol{U}) - \boldsymbol{F}_{j-1/2}(\boldsymbol{U})] + \frac{\Delta t^{1/2}}{\Delta x^{3/2}} (\boldsymbol{Z}_{j+1/2} - \boldsymbol{Z}_{j-1/2}).
$$

Each time step of the RK3 algorithm is composed of three stages

$$
\boldsymbol{U}_j^{n+1/3} = \boldsymbol{U}_j^n + \Delta \boldsymbol{U}_j(\boldsymbol{U}^n, \boldsymbol{W}_1) \qquad \text{(estimate at } t = (n+1)\Delta t),
$$

$$
\boldsymbol{U}_j^{n+2/3} = \tfrac{3}{4} \boldsymbol{U}_j^n + \tfrac{1}{4} [\boldsymbol{U}_j^{n+1/3} + \Delta \boldsymbol{U}_j(\boldsymbol{U}_j^{n+1/3}, \boldsymbol{W}_2)] \quad \text{(estimate at } t = (n+\tfrac{1}{2})\Delta t), \quad (60)
$$

$$
\boldsymbol{U}_j^{n+1} = \tfrac{1}{3} \boldsymbol{U}_j^n + \tfrac{2}{3} [\boldsymbol{U}_j^{n+2/3} + \Delta \boldsymbol{U}_j(\boldsymbol{U}^{n+2/3}, \boldsymbol{W}_3)],
$$

where for now we have not assumed anything about how the stochastic fluxes between different stages, $\boldsymbol{W}_1$, $\boldsymbol{W}_2$ and $\boldsymbol{W}_3$, are related to each other. The relevant dimensionless parameters that measure the ratio of the time step to the CFL stability limits are

$$
\alpha = \frac{c_0 \Delta t}{\Delta x}, \quad \beta = \frac{\eta_0 \Delta t}{\rho_0 \Delta x^2} = \frac{\alpha}{r}, \quad \beta_T = \frac{\mu_0 \Delta t}{\rho_0 c_v \Delta x^2} = \frac{1}{\mathrm{Pr}} \frac{\alpha}{r} = \frac{\alpha}{p},
$$

where $r = c_0 \rho_0 \Delta x / \eta_0$ is the cell Reynolds number (we have assumed a low Mach number flow, that is, $|v_0| \ll c_0$), and $\mathrm{Pr} = \eta_0 c_v / \mu_0$ is the Prandtl number of the fluid. For low-density gases, r and $p = r\mathrm{Pr}$ can be close to or smaller than one; however, for dense fluids sound dominates and $r > 1$ and $p > 1$ for all reasonable

Δx (essentially, $\Delta x > \lambda$, where λ is the mean free path). In practice, in order to fully resolve viscous scales, one should keep both r and p reasonably small.

6B. *Evaluation of the stochastic fluxes.* In the original RK3 algorithm [13], a different stochastic flux is generated in each stage, that is, $W_s = \sqrt{2} W_{RNG}^{(s)}$, $s = 1, 2, 3$. The additional prefactor $\sqrt{2}$ is added because the averaging between the three stages reduces the variance of the overall stochastic flux. One can also use different weights for each of the three stochastic fluxes, that is, $W_s = w_s W_{RNG}^{(s)}$. Another option is to simply use the same stochastic flux $W_{RNG}^{(0)}$ in all three stages, that is, $W_s = W_{RNG}^{(0)}$. A further option is to use the same random flux $W_{RNG}^{(0)}$ in all three stages, but put in different weights in each stage, that is, $W_s = w_s W_{RNG}^{(0)}$. Our goal is to find out which approach is optimal. For this purpose, we can generally assume that the three random fluxes are different, to obtain a total of six random numbers per cell per step, and use the formalism developed in Section 3 with $N_s = 6$ to express the structure factor in terms of the 6×6 covariance matrix of the random variates. This calculation is too tedious even for a computer algebra system, and we therefore first study the simple advection-diffusion Equation (35) in order to gain some insight.

6B1. *Advection-diffusion equation.* The RK3 method can be directly applied to the scalar advection-diffusion equation in one dimension (52). Experience with deterministic solvers suggests that a numerical scheme that performs well on this type of model equation is likely to perform well on the full system (1) when viscous effects are fully resolved. Here we use PPM-interpolation based discretization of the hyperbolic flux given in (59), which leads to a standard fourth-order centered difference approximation to the first derivative v_x [9], and thus justifies our choice for the interpolation. We discretize the gradient used in calculating the diffusive fluxes using the second-order centered difference

$$\nabla_{j+1/2} u = \frac{u_{j+1} - u_j}{\Delta x},$$

which leads to the standard second-order centered difference approximation to the second derivative v_{xx} (the challenges with using the standard fourth-order centered difference approximation to v_{xx} [9] are discussed in Section 5C). The stencil widths in (23) are $w_D = 6$ (three stages with stencil width two each) and $w_S = 4$, and there are $N_s = 3$ random numbers per cell per step (one per stage), with a general 3×3 covariance matrix C_W. Equation (27) can then be solved to obtain the static structure factor for any wavenumber, however, these expressions are too complex to be useful for analysis. Instead, we perform an expansion of both sides of (27) for small k and thus focus on the behavior of the static structure factors for small wavenumbers and small time steps.

As a first condition on C_W, we have the weak consistency requirement $S_{k=0} = 1$. With this condition satisfied, the method satisfies the discrete fluctuation-dissipation

balance in the limit $\Delta t \to 0$ since the discretization of the divergence is the negative adjoint of the discretization of the gradient. A second condition is obtained by equating the coefficient in front of the leading-order error term in S_k, of order $\alpha \Delta k^2$, to zero; where the advective dimensionless CFL number is $\alpha = a\Delta t/\Delta x$. It turns out that this also makes the term of order $\alpha \Delta k^4$ vanish. A third condition is obtained by equating the coefficient in front of the next-order error term of order $\alpha^2 \Delta k^2$ to zero. Finally, a fourth condition equates the coefficient in front of $\alpha^2 \Delta k^4$ to zero. For this three-stage method, it is not possible to make the terms with higher powers of α vanish identically for any choice of C_W. No additional conditions are obtained by looking at terms with powers of the diffusive CFL number $\beta = \mu \Delta t/\Delta x^2$ since, as it turns out, the accuracy is always limited by the hyperbolic fluxes.

The various ways of generating the stochastic fluxes can now be compared by investigating how many of these conditions are satisfied. It turns out that only the first condition is satisfied if we use a different independently generated stochastic flux in each stage (one can satisfy one more condition by using different weights for the three independent stochastic fluxes). The second condition is satisfied if we use the same stochastic flux in all stages with a unit weight, that is, $W_s = w_s W_{RNG}^{(0)}$ with $w_1 = w_2 = w_3 = 1$. Armed with the freedom to put a different weight for this flux in each of the stages, we can satisfy the third condition as well if we use

$$w_1 = \tfrac{3}{4}, \quad w_2 = \tfrac{3}{2}, \quad w_3 = \tfrac{15}{16}, \tag{61}$$

which gives a structure factor

$$S_k = 1 - \frac{r}{24}\alpha^3 \Delta k^2 - \frac{1}{6r^2}\alpha^2 \Delta k^4 + \text{h.o.t.}$$

If we are willing to increase the cost of each step and generate two random numbers per cell per step, we can satisfy the fourth condition as well. For this purpose, we look for a covariance matrix C_W that satisfies the four conditions and is also positive semidefinite and has a rank of two, that is, has a smallest eigenvalue of zero. A solution to these equations gives the following method for evaluating the stochastic fluxes in the three stages

$$W_1 = W_{RNG}^{(A)} - \sqrt{3}W_{RNG}^{(B)}, \quad W_2 = W_{RNG}^{(A)} + \sqrt{3}W_{RNG}^{(B)}, \quad W_3 = W_{RNG}^{(A)}, \tag{62}$$

where $W_{RNG}^{(A)}$ and $W_{RNG}^{(B)}$ are two independent random vectors that need to be generated and stored during each RK3 step. This approach produces a structure factor

$$S_k = 1 - \frac{r}{24}\alpha^3 \Delta k^2 - \frac{24+r^2}{288r}\alpha^3 \Delta k^4 + \text{h.o.t.}$$

We will refer to the RK3 scheme that uses one random flux per step and the weights in (61) as the *RK3-1RNG scheme*, and to the RK3 scheme with two random fluxes per step as given in (62) as the *RK3-2RNG scheme*.

It is important to point out that for the MacCormack method, which is equivalent to the Lax–Wendroff method for the advection-diffusion equation, the leading-order errors are of order $\alpha \Delta k^2$. This is much worse than for the stochastic heat equation (see Section 5A) even though the MacCormack scheme is a predictor-corrector method. This is because of the low-order handling of advective fluxes used in the MacCormack method to stabilize the two-stage Runge–Kutta time integrator.

6C. *Results for LLNS equations in one dimension.* We can now theoretically study the behavior of the RK3-1RNG and RK3-2RNG schemes on the full linearized system (56), specializing to the case of zero background flow, $v_0 = 0$. As expected, we find that the behavior is very similar to the one observed for the advection-diffusion equation; in particular, the leading order terms have the same basic form. Specifically, the expansions of the diagonal and off-diagonal components of the structure factor $\boldsymbol{S}_k$ for the RK3-1RNG method are

$$S_k^{(\rho)} \approx S_k^{(T)} \approx 1 + \frac{S_k^{(u)} - 1}{3} \approx 1 + \varepsilon(\alpha)\Delta k^2,$$

$$S_k^{(\rho,u)} \approx \frac{i}{12r}\alpha^2 \Delta k^3,$$

$$S_k^{(\rho,T)} \approx 2\varepsilon(\alpha)\Delta k^2,$$

$$S_k^{(u,T)} \approx i\frac{r-p}{6pr}\alpha^2 \Delta k^3,$$

(63)

where

$$\varepsilon(\alpha) = -\frac{3\alpha^3 pr}{4(3p+2r)}.$$

These structure factors are shown in Figure 2 for sample discretization parameters, along with the corresponding results for RK3-2RNG. We see from these expressions that as the speed of sound dominates the stability restrictions on the time step more and more, namely, as p or r become larger and larger, a smaller α is required to reach the same level of accuracy, that is, a smaller time step relative to the acoustic CFL stability limit is required.

Similar results to Equation (63) hold also for the isothermal LLNS equations (in which the there is no energy equation), for which the calculations are simpler. For linearization around a constant background flow of speed $v_0 = c_0\text{Ma}$, where Ma is the reference Mach number, the analysis for the isothermal LLNS equations shows that the error grows with the Mach number as

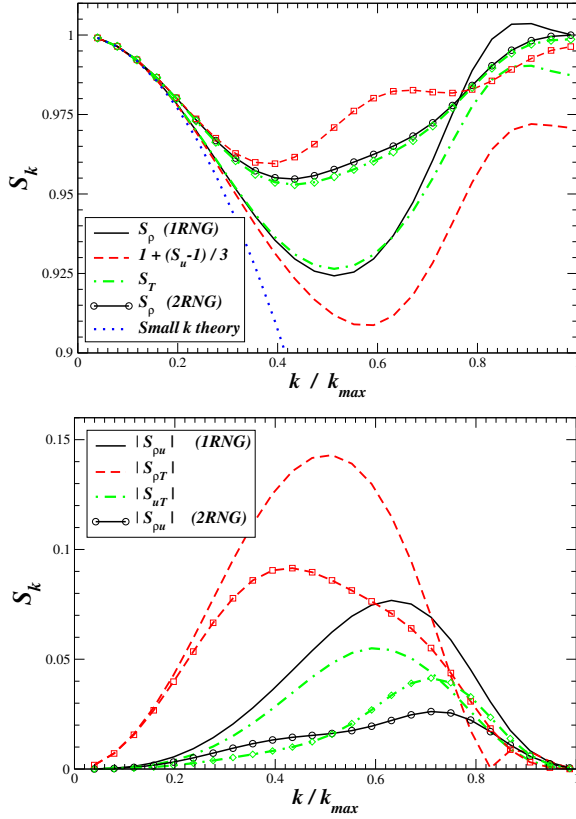$$S_k^{(\rho)} \approx 1 + \varepsilon(\alpha)[1 + 6\text{Ma}^2 + \text{Ma}^4]\Delta k^2.$$

Figure 2. Discrete structure factor S_k for the LLNS equation under the RK3-1RNG (lines) and RK3-2RNG (same style of lines with added symbols) schemes, as calculated by numerical solution of (27) for an ideal one-dimensional gas, for $\alpha = 0.5$, $\beta = 0.2$ and $\beta_T = 0.1$. Left: diagonal (self) structure factors, which should ideally be identically unity. Also shown is the leading order error term $1 + \varepsilon(\alpha)\Delta k^2$ (dotted line), which is the same for both schemes. Right: off-diagonal (cross) structure factors, which should ideally be identically zero.

7. Higher dimensions

Much of what we already described for one dimension applies directly to higher dimensions [13; 10]. However, there is a peculiarity with the LLNS equations in three dimensions that does not appear in one dimension, and also does not appear for the scalar diffusion equation [6]. In one dimension the velocity component of the LLNS system of equations is essentially an advection-diffusion equation. In higher dimensions, however, there is an important difference: namely, the dissipation

operator is a *modified* Laplacian $\mathcal{L}_m$. By neglecting the hyperbolic coupling between velocity and the other variables in the linearized LLNS equations, we obtain the *stochastic diffusion equation*

$$
\begin{aligned}
\vartheta_t &= \eta \nabla \cdot [C (\nabla \vartheta)] + \sqrt{2\eta} \nabla \cdot [C^{1/2} \mathcal{W}] \\
&= \eta \left(\mathcal{D} C \mathcal{G}\right) \vartheta + \sqrt{2\eta} \mathcal{D} C^{1/2} \mathcal{W} = \eta \mathcal{L}_m \vartheta + \sqrt{2\eta} \mathcal{W}_m,
\end{aligned}
\tag{64}
$$

where C is the linear operator that transforms the velocity gradient into a traceless symmetric stress tensor

$$
C (\nabla \vartheta) = 2\left[\tfrac{1}{2}(\nabla \vartheta + \nabla \vartheta^T) - \tfrac{1}{3} I \, (\nabla \cdot \vartheta)\right],
\tag{65}
$$

and we have denoted the continuum velocity field by $\vartheta \equiv \mathcal{U}$ in order to distinguish from the discretized velocities $v \equiv U$. Here we will focus on two-dimensional flows, $\vartheta = [\vartheta_x, \vartheta_y]$, however, identical considerations apply to the fully three-dimensional case.

If we arrange the components of the velocity gradient as a vector with four components, $\nabla \vartheta = [\partial_x \vartheta_x, \partial_x \vartheta_y, \partial_y \vartheta_x, \partial_y \vartheta_y]^T$, the linear operator C in (65) becomes the matrix

$$
C = \begin{bmatrix}
\tfrac{4}{3} & 0 & 0 & -\tfrac{2}{3} \\
0 & 1 & 1 & 0 \\
0 & 1 & 1 & 0 \\
-\tfrac{2}{3} & 0 & 0 & \tfrac{4}{3}
\end{bmatrix},
\tag{66}
$$

which is not diagonal. This means that the components of the stochastic stress $C^{1/2} W$ would need to have nontrivial correlations between the x fluxes for v_x and y fluxes for v_y, as well as between the x fluxes for v_y and y fluxes for v_x. These correlations essentially amount to the requirement that the stochastic stress be a traceless symmetric tensor, at least at the level of its covariance matrix. Numerically, one generates independent random variates for the upper triangular portion of the stochastic stress tensor for each cell, then makes the tensor traceless and symmetric [28]. Note that one can save one random number by using only $d - 1$ variates to generate the diagonal elements.

However, it is important to point out that an *equivalent* formulation is obtained by using the operator

$$
C = \begin{bmatrix}
\tfrac{4}{3} & 0 & 0 & \tfrac{1}{3} \\
0 & 1 & 0 & 0 \\
0 & 0 & 1 & 0 \\
\tfrac{1}{3} & 0 & 0 & \tfrac{4}{3}
\end{bmatrix} = I + \begin{bmatrix}
\tfrac{1}{3} & 0 & 0 & \tfrac{1}{3} \\
0 & 0 & 0 & 0 \\
0 & 0 & 0 & 0 \\
\tfrac{1}{3} & 0 & 0 & \tfrac{1}{3}
\end{bmatrix},
\tag{67}
$$

where there is nontrivial cross correlations only between the x fluxes for v_x and y fluxes for v_y. The splitting of the operator C in (67) corresponds to rewriting the

stochastic diffusion Equation (64) in the equivalent but suggestive form

$$\vartheta_t = -\eta\big[\nabla^2\vartheta + \tfrac{1}{3}\nabla\left(\nabla\cdot\vartheta\right)\big] + \sqrt{2\eta}\big[(\nabla\cdot\boldsymbol{\mathcal{W}}_T) + \sqrt{\tfrac{1}{3}}\nabla\mathcal{W}_V\big]$$

$$-= \eta\big(\boldsymbol{\mathcal{D}}_T\boldsymbol{\mathcal{G}}_T + \tfrac{1}{3}\boldsymbol{\mathcal{G}}_V\boldsymbol{\mathcal{D}}_V\big)\vartheta + \sqrt{2\eta}\big(\boldsymbol{\mathcal{D}}_T\boldsymbol{W}_T + \sqrt{\tfrac{1}{3}}\boldsymbol{\mathcal{G}}_V\mathcal{W}_V\big), \qquad (68)$$

where we have now distinguished between the *tensorial* divergence $\boldsymbol{\mathcal{D}}_T$ and gradient operators $\boldsymbol{\mathcal{G}}_T = -\boldsymbol{\mathcal{D}}_T^\star$, which map from tensor to vector fields and vector to tensor fields, respectively, and the *vectorial* divergence $\boldsymbol{\mathcal{D}}_V$ and gradient operators $\boldsymbol{\mathcal{G}}_V = -\boldsymbol{\mathcal{D}}_V^\star$, which map from vector to scalar fields and scalar to vector fields, respectively. Corresponding to the splitting of the modified Laplacian $\boldsymbol{\mathcal{L}}_m = \boldsymbol{\mathcal{D}}C\boldsymbol{\mathcal{G}} = \boldsymbol{\mathcal{L}}_T + \boldsymbol{\mathcal{L}}_V$ into the tensorial Laplacian operator $\boldsymbol{\mathcal{L}}_T = \boldsymbol{\mathcal{D}}_T\boldsymbol{\mathcal{G}}_T$ and the vectorial component $\boldsymbol{\mathcal{L}}_V = \boldsymbol{\mathcal{G}}_V\boldsymbol{\mathcal{D}}_V/3$, in (68) we have split the stochastic stress into a tensor white-noise field $\boldsymbol{\mathcal{W}}_T$ in which all components are uncorrelated, and a scalar white-noise field $\mathcal{W}_V$, which we will call the stochastic *divergence stress*. This representation is perhaps more physically intuitive than the standard formulation in which the stochastic stress has unexpected exact symmetry and is exactly traceless. Note that in the more general case where the diffusion coefficient is spatially dependent and there is nonzero bulk viscosity η_B, the dissipative term in (68) becomes

$$\nabla\cdot[\eta(\nabla\vartheta)] + \nabla[(\eta/3 + \eta_B)\nabla\cdot\vartheta],$$

with an equivalent change in the stochastic term. Also note that for the fluctuating incompressible Navier–Stokes equation the term with the velocity divergence disappears and the dissipation operator is a projected traditional Laplacian [8; 5], while the stochastic flux is simply a projected tensor white-noise field.

7A. *Discrete fluctuation dissipation balance.* Our ultimate goal is to find a scheme that satisfies the discrete fluctuation dissipation theorem, that is, find a discrete modified Laplacian $\boldsymbol{L}_m$ that is a consistent approximation to the continuum modified Laplacian $\boldsymbol{\mathcal{L}}_m(\boldsymbol{k})\widehat{\vartheta} = \boldsymbol{k}\cdot[\boldsymbol{C}(\boldsymbol{k}\widehat{\vartheta}^T)]$ for small k, and a way to efficiently generate random increments $\boldsymbol{W}_m$ that discretize $\boldsymbol{\mathcal{W}}_m$ and whose covariance is $\langle\boldsymbol{W}_m\boldsymbol{W}_m^\star\rangle = \boldsymbol{L}_m$. This task is nontrivial in general, and completing it requires some ingenuity and insight, as illustrated in the work of Atzberger [6] on multigrid methods for the scalar stochastic diffusion equation. We illustrate two different approaches next, the first corresponding to attempting to directly discretize the modified Laplacian $\boldsymbol{\mathcal{L}}_m$, and the second corresponding to discretizing the split Laplacian $\boldsymbol{\mathcal{L}}_T + \boldsymbol{\mathcal{L}}_V/3$. In the continuum context these are, of course, equivalent, but this is not the case in the discrete context. Namely, in the continuum formulation, C maps from gradients to stresses, the divergence operator $\boldsymbol{\mathcal{D}}$ maps from fluxes to fields, and the gradient $\boldsymbol{\mathcal{G}}$ maps from fields to gradients. In the continuum context, stresses, gradients and fluxes are all tensor fields and thus in the same Hilbert space. In the discrete

context, however, stresses, gradients and fluxes may be discretized differently and thus belong to different spaces.

7A1. *The modified Laplacian approach.* One approach to the problem of constructing discrete operators that satisfy the discrete fluctuation-dissipation balance is to find a discretization of the divergence D and gradient G operators that are skew-adjoint and then form the modified Laplacian $L_m = DCG = -DCD^\star$, and generate the stochastic increments as $W_m = DC^{1/2}W$. As discussed above, for the meaning of $C^{1/2}$ to be clear, stresses and gradients must belong to the same space. Furthermore, it is required that the discrete operators D and G be skew adjoint so that the discrete fluctuation dissipation balance condition (31) is satisfied.

The issue of how to define skew adjoint D and G operators also arose in the historical development of projection algorithms for incompressible flow. The incompressible flow literature suggests two approaches that discretize both gradients and stresses by representing them with tensors at the same grid of points. The first approach corresponds to fully cell-centered discretization originally proposed by Chorin [17], which uses centered differences to define a skew-adjoint gradient and divergence operators. The second approach corresponds to a finite element-based discretization developed by Fortin [31] and later used in the projection algorithm of Bell et al. [11].

In the Fortin approach both stresses and gradients are represented as $d \times d$ tensors at the corners of a regular grid, where d is the spatial dimension. The divergence operator D combines the values of the stresses at the $2d$ corners of a cell to produce a value at the center of the cell. The gradient $G = -D^\star$ combines the values of the fields at the centers of the $2d$ cells that share a corner into a gradient at that corner. In this scheme, the stochastic stresses also live at the corners of the grid. They are generated to have the required covariance, for example, (66). Unfortunately, the discrete Fortin Laplacian $L = DG$ suffers from a serious drawback: it has a nontrivial null space. For example, for the scalar heat equation on a uniform grid in two dimensions, the Laplacian stencil obtained from the Fortin discretization is

$$(L^{(F)}u)_{i,j} = \Delta x^{-2}\left[\tfrac{1}{2}(u_{i+1,j+1} + u_{i-1,j+1} + u_{i-1,j-1} + u_{i+1,j-1}) - 2u_{i,j}\right],$$

for which the odd ($i + j$ odd) and even ($i + j$ even) points on the grid are completely decoupled. In Fourier space the above Laplacian is $-2[1 - \cos(\Delta k_x)\cos(\Delta k_y)]$ and thus vanishes for the largest wavevectors, $|\Delta k_x| = \pi$, $|\Delta k_y| = \pi$, which correspond to checker board zero eigenmodes.

It can easily be verified that the same type of checker board zero eigenmodes also exist for the modified Fortin Laplacian $L_m = DCG$. In three dimensions, there are $O(N)$ zero eigenmodes for a grid of size N^3. Issues arising when using these types of stencils in the deterministic context are discussed in Almgren et al. [3]. Our theory for the structure factor implicitly relies on the definiteness of the

discrete generator, and in fact, in the general nonlinear setting the zero modes lead to instabilities of the solution of the full LLNS system of equations. We therefore abandon the Fortin corner-centered discretization of the fluxes.

Fully cell-centered approximations to D and G based on second-order centered differences, previously studied in the context of projection methods for incompressible flows by Chorin [17], lead to a discrete Laplacian that also has a nontrivial null space and suffers similar shortcomings as the Fortin Laplacian. Specifically, even in one dimension one obtains a Laplacian stencil

$$(L^{(C)}u)_i = \frac{1}{4\Delta x^2}[u_{i-2} - 2u_i + u_{i+2}],$$

where the odd-even decoupling is evident. Here we develop a cell-centered (collocated) discretization that preserves the null space of the continuum Laplacian.

7A2. *The split Laplacian approach.* An alternative to trying to form a discrete modified Laplacian $L_m = L_T + L_V$ directly is to use the splitting in (68) and form the discrete tensorial $L_T = D_T G_T$ and vectorial $L_V = G_V D_V/3$ components separately from discretizations of the tensorial and vectorial divergence and gradient operators that are skew-adjoint, $G_T = -D_T^\star$ and $G_V = -D_V^\star$. The stochastic increments would simply be generated as $D_T W_T + G_V W_V/\sqrt{3}$, where W_V and the components of W_T are independent normal variates.

A popular approach to discretizing the tensorial divergence and gradient operators, commonly referred to as a MAC discretization in projection algorithms for incompressible flow [38], defines a divergence at cells centers from normal fluxes on edges, with a corresponding gradient that gives normal derivatives at cell edges from cell-centered values:

$$(DZ)_{i,j} = \Delta x^{-1}(Z_{i+1/2,j}^{(x)} - Z_{i-1/2,j}^{(x)}) + \Delta y^{-1}(Z_{i,j+1/2}^{(y)} - Z_{i,j-1/2}^{(y)}) \to \nabla \cdot Z,$$
$$-(D^\star v)_{i+1/2,j} = \Delta x^{-1}(v_{i+1,j} - v_{i,j}) \to \partial v/\partial x, \qquad (69)$$
$$-(D^\star v)_{i,j+1/2} = \Delta y^{-1}(v_{i,j+1} - v_{i,j}) \to \partial v/\partial y.$$

In this discretization, the tensor field

$$Z = [Z^{(x)}; Z^{(y)}] = [Z_{v_x}^{(x)}, Z_{v_y}^{(x)}; Z_{v_x}^{(y)}, Z_{v_y}^{(y)}]$$

is strictly divided into an x vector $Z^{(x)}$, which is represented on the x faces of the grid, and a y vector $Z^{(y)}$, represented on the y faces of the grid. The MAC discretization, which we used in the earlier one-dimensional examples, leads to a standard 5 point discrete Laplacian in two dimensions (3 point in one dimension, 7 point in three dimensions),

$$(L^{(\text{MAC})}u)_{i,j} = [\Delta x^{-2}(u_{i-1,j} - 2u_{i,j} + u_{i+1,j}) + \Delta y^{-2}(u_{i,j-1} - 2u_{i,j} + u_{i,j+1})].$$

In Fourier space the MAC Laplacian is $2\cos(\Delta k_x) + 2\cos(\Delta k_y) - 4$ and is strictly negative for all nonzero wavevectors, and thus does not suffer from the instabilities of the Chorin and Fortin discrete Laplacians, discussed in Section 7A1.

The vectorial divergence and gradient operators cannot be discretized using the MAC framework. Namely, $\boldsymbol{D}_V$ must operate on a cell-centered vector field $\boldsymbol{v}$, whereas the MAC-type discretization operates on face-centered values. Instead, for the vectorial component we can use either the Chorin discretization [17], in which both scalar and vector fields are cell-centered, or the Fortin discretization [31], in which scalar fields are represented at corners and vector fields are cell-centered. Here we choose the Fortin discretization and calculate a (scalar-valued) velocity divergence and the corresponding divergence stress at the corners of the grid, and also generate a (scalar) random divergence stress at each corner. The deterministic and random components are added to form the total corner-centered divergence stress, and the velocity increment is calculated from the (vector-valued) cell-centered gradient of the divergence stresses. Note that the nontrivial nullspace of $\boldsymbol{L}_V$ does not pose a problem since $\boldsymbol{L}_T$ and thus also $\boldsymbol{L}_m = \boldsymbol{L}_T + \boldsymbol{L}_V$ has a trivial nullspace.

The discrete modified Laplacian that is obtained by this mixed MAC/Fortin discretization can be represented in terms of second-order centered-difference stencils. The first (i.e., the v_x) component of this Laplacian can be represented as a linear combination of the velocities in the 9 neighboring cells:

$$(\boldsymbol{L}_m \boldsymbol{v})_{jk}^{(v_x)} = \sum_{l,m=-1}^{1} \left(\frac{1}{\Delta x^2} L_{2-m,2+l}^{(\mathrm{MAC},x)} v_{j+l,k+m}^{(x)} + \frac{1}{\Delta y^2} L_{2-m,2+l}^{(\mathrm{MAC},y)} v_{j+l,k+m}^{(x)} \right.$$
$$\left. + \frac{1}{3\Delta x^2} L_{2-m,2+l}^{(F,x)} v_{j+l,k+m}^{(x)} + \frac{1}{3\Delta x \Delta y} L_{2-m,2+l}^{(F,xy)} v_{j+l,k+m}^{(y)} \right), \quad (70)$$

where $\boldsymbol{L}^{(\mathrm{MAC},x/y)}$ and $\boldsymbol{L}^{(F,x/y)}$ correspond to a second-order MAC and Fortin discretizations of the terms $\partial_{xx}\vartheta_x$ and $\partial_{yy}\vartheta_y$ respectively, and $\boldsymbol{L}^{(F,xy)}$ discretizes $\partial_{xy}\vartheta_y$. The same stencils apply to the second (i.e., the v_y) component of the Laplacian as well, by symmetry:

$$(\boldsymbol{L}_m \boldsymbol{v})_{jk}^{(v_y)} = \sum_{l,m=-1}^{1} \left(\frac{1}{\Delta x^2} L_{2-m,2+l}^{(\mathrm{MAC},x)} v_{j+l,k+m}^{(y)} + \frac{1}{\Delta y^2} L_{2-m,2+l}^{(\mathrm{MAC},y)} v_{j+l,k+m}^{(y)} \right.$$
$$\left. + \frac{1}{3\Delta y^2} L_{2-m,2+l}^{(F,y)} v_{j+m,k+l}^{(y)} + \frac{1}{3\Delta x \Delta y} L_{2-m,2+l}^{(F,xy)} v_{j+m,k+l}^{(x)} \right). \quad (71)$$

Note that we chose the peculiar indexing of the stencils so that when printed on paper they correspond to the usual Cartesian representation of the x-y grid. The

coefficients of the MAC stencil (70) are

$$\boldsymbol{L}^{(\mathrm{MAC},x)} = \begin{bmatrix} 0 & 0 & 0 \\ 1 & -2 & 1 \\ 0 & 0 & 0 \end{bmatrix} \quad \text{and} \quad \boldsymbol{L}^{(\mathrm{MAC},y)} = \begin{bmatrix} 0 & 1 & 0 \\ 0 & -2 & 0 \\ 0 & 1 & 0 \end{bmatrix}, \quad (72)$$

while the Fortin stencils are

$$\boldsymbol{L}^{(F,x)} = \begin{bmatrix} \frac{1}{4} & -\frac{1}{2} & \frac{1}{4} \\ \frac{1}{2} & -1 & \frac{1}{2} \\ \frac{1}{4} & -\frac{1}{2} & \frac{1}{4} \end{bmatrix}, \quad \boldsymbol{L}^{(F,y)} = \begin{bmatrix} \frac{1}{4} & \frac{1}{2} & \frac{1}{4} \\ -\frac{1}{2} & -1 & -\frac{1}{2} \\ \frac{1}{4} & \frac{1}{2} & \frac{1}{4} \end{bmatrix},$$

$$\boldsymbol{L}^{(F,xy)} = \begin{bmatrix} -\frac{1}{4} & 0 & \frac{1}{4} \\ 0 & 0 & 0 \\ \frac{1}{4} & 0 & -\frac{1}{4} \end{bmatrix}. \quad (73)$$

7B. *Results in three dimensions.* Our theoretical calculations have helped in formulating a complete three-stage Runge–Kutta scheme for solving the full LLNS system in one, two or three spatial dimensions. We have discussed how to generate stochastic fluxes in each stage, including the required correlations among the components of the stochastic stress, and have also discussed how to relate the stochastic fluxes in each stage. Since theoretical calculation of the three-dimensional structure factors is out of reach, we present some numerical results for the RK3-2RNG method in three dimensions with the mixed MAC/Fortin handling of the split Laplacian as given in Equations (70) and (71), hereafter termed the *RK3D-2RNG algorithm*.

We note in passing that it is also possible to discretize the modified Laplacian (see Section 7A1) using a MAC-like discretization of the viscous and stochastic stresses that avoids the use of the Fortin corner-based discretization of the divergence stress. This saves one random number per cell per stochastic flux, however, it requires the use of a nonstandard randomized cell-to-face projection (splitting) of the stochastic stresses that complicates the analysis and handling of physical boundaries and makes parallelization more difficult. We therefore do not describe this approach here, and only note that it produces very similar structure factors to those reported here.

We focus on the behavior of the scheme in global equilibrium with periodic boundary conditions. We have implemented the full nonlinear fluxes as proposed in [13; 10], using the interpolation in (59) for the hyperbolic fluxes and simple interpolation of the spatially varying viscosity and thermal conductivity in the handling of the viscous and stochastic fluxes. However, in the tests reported here we have made the magnitude of the fluctuations small compared to the means to ensure that the behavior is very similar to the linearized LLNS equations. Including the full

nonlinear system guarantees conservation and ensures that there are no nonlinearly unstable modes. More careful study of the proper handling of nonlinearity in the LLNS equations themselves and the associated numerical solvers is deferred to future publications; here, we focus on verification that the nonlinear scheme produces behavior consistent with the linearized analysis. We note that we have implemented the new RK3D algorithm also for the LLNS equations for a mixture of two ideal gases, closely following the original scheme described in [10]. We find that the spatial discretization satisfies the discrete fluctuation-dissipation balance even in the presence of concentration as an additional primitive variable and that the RK3D-2RNG method performs very well with reasonably large time steps.

7B1. *Static structure factors.* Examples of static structure factor S_k for the RK3D-2RNG scheme are shown in Figure 3, showing that the diagonal components $S_k^{(\rho)}$, $S_k^{(v_x)}$, and $S_k^{(T)}$ are close to unity, while the off-diagonal components $S_k^{(\rho, v_x)}$, $S_k^{(v_x, v_y)}$, and $S_k^{(\rho, T)}$ are close to zero (similar results hold for $S_k^{(v_x, T)}$, not shown), even for a large time step (half of the stability limit). Note that the static structure factor is difficult to obtain accurately for the smallest wavenumbers (slowest modes) and therefore the values near the centers of the k-grid should be ignored.

It is seen in the figures that the diagonal components of S_k are quite close to unity for the largest wavevectors, which is somewhat surprising, and the largest error is actually seen for intermediate wavenumbers, consistent with the one-dimensional results shown in Figure 2. We have tested the method on several cell Reynolds numbers r and found that the results are worse as r increases, consistent with the previous analysis, however, the higher order of temporal accuracy allows for increasing the time step to be a reasonable fraction of the stability limit even for large r.

These results represent a significant improvement over the results obtained for the original RK3 scheme presented in Bell et al. [13; 10]. Results with the original scheme were sensitive to time steps, requiring small time steps to obtain satisfactory results; the new scheme produces satisfactory results for time steps near the stability limit. Also, through the use of the mixed MAC and Fortin discretization, the new scheme eliminates a weak but spurious correlation $S_k^{(v_x, v_y)}$ present in the original scheme for small wavenumbers even in the limit of small time steps.

7B2. *Dynamic structure factors.* Examples of dynamic structure factors $S_{k,\omega}$ for the RK3D-2RNG scheme are shown in Figure 4 as a function of ω for two relatively large wavevectors, along with the correct continuum result obtained by solving the system (4) through a space-time Fourier transform (we did not make any of the usual approximations made in analytical calculations of $S_{k,\omega}$ [20], and instead used Maple's numerical linear algebra). It is well known that $S_{k,\omega}^{(\rho)}$ and $S_{k,\omega}^{(T)}$ exhibit three peaks for a given k [20], one central Rayleigh peak at $\omega = 0$ similar to the

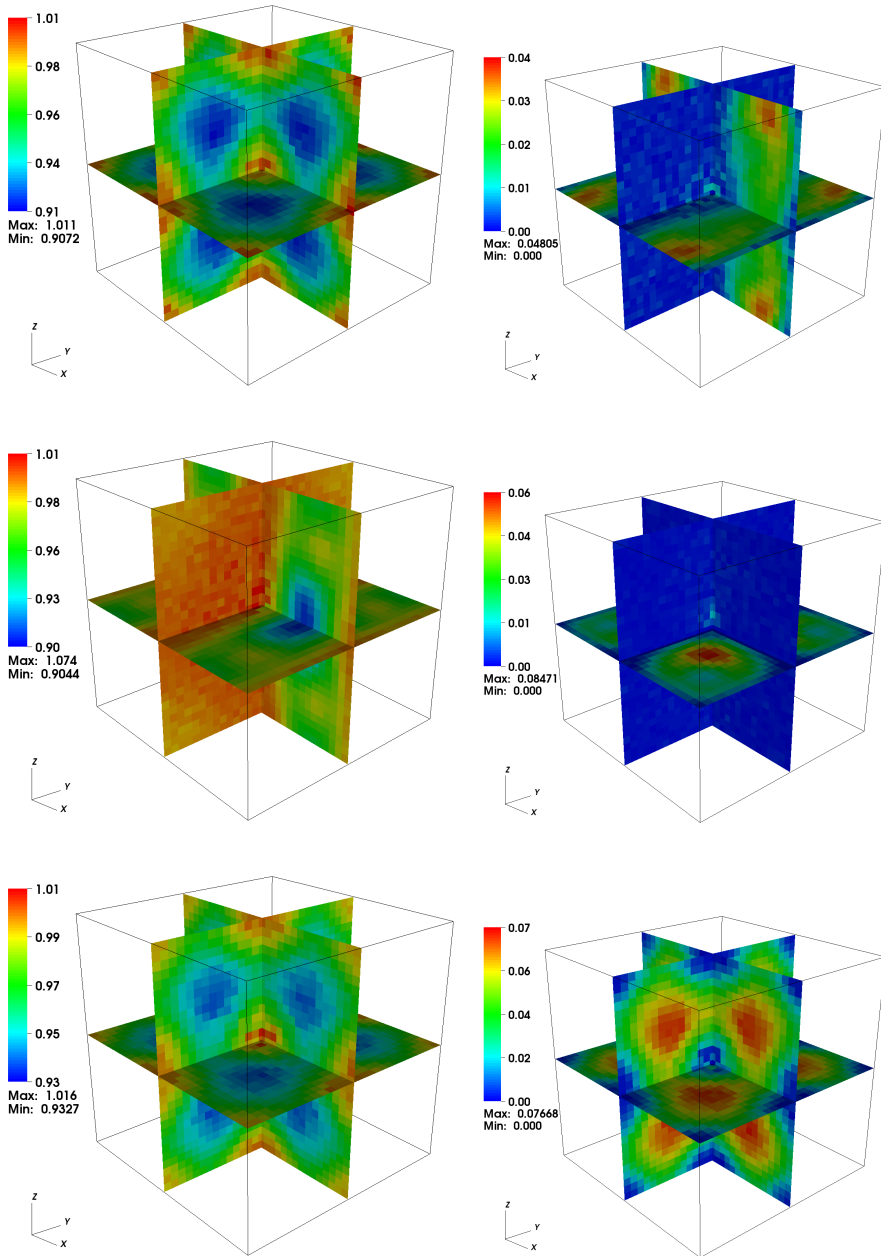**Figure 3.** Left: $S_{\boldsymbol{k}}^{(\rho)}$, $S_{\boldsymbol{k}}^{(v_x)}$, and $S_{\boldsymbol{k}}^{(T)}$ (top to bottom). Right: $|S_{\boldsymbol{k}}^{(\rho,v_x)}|$, $|S_{\boldsymbol{k}}^{(v_x,v_y)}|$ and $|S_{\boldsymbol{k}}^{(\rho,T)}|$ (top to bottom) for RK3D-2RNG (random direction), with the time step $\alpha = 0.5$, $\beta = 3\beta_T/2 = 0.1$, periodic boundary conditions with 30^3 cells, and averaging over 10^6 time steps.
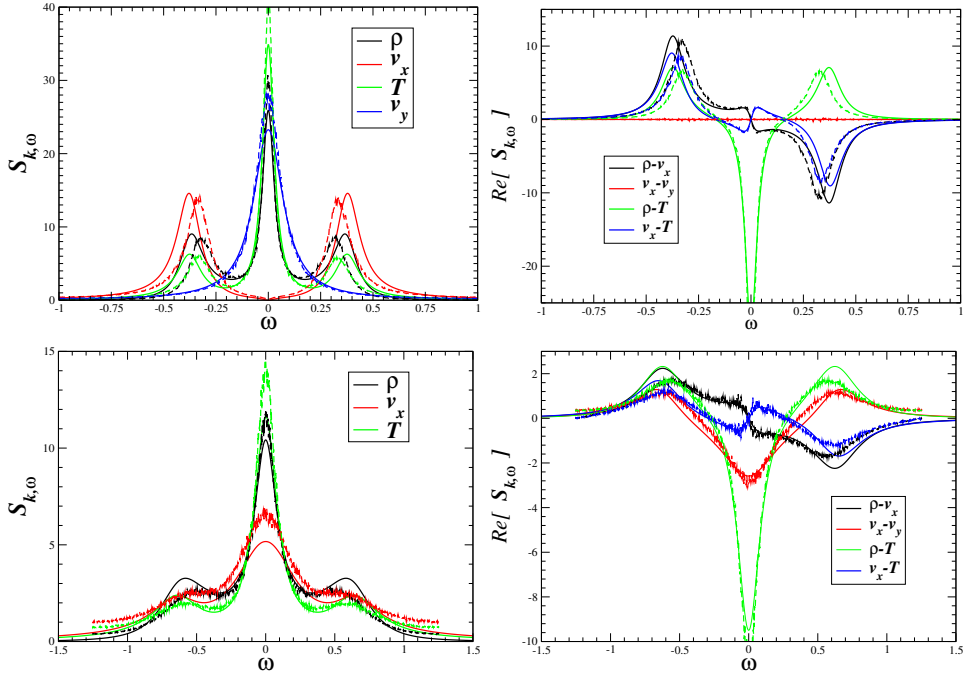
Figure 4. Diagonal (left) and the real part of the off-diagonal (right) components of the dynamic structure factor $S_{k,\omega}$ for RK3D-2RNG (dashed lines) for the same parameters as in Figure 3. For comparison, the analytical solution of the LLNS equations in Fourier space are also shown (solid lines). The imaginary part of the off-diagonal components is less than 0.1 and it vanishes in the theory. The top part shows the wavevector $k =(k_{\max}/2, 0, 0)$ and the bottom shows $k =(k_{\max}/2, k_{\max}/2, k_{\max}/2)$.

peak for the diffusion equation given in (43), and two symmetric Brillouin peaks at $\omega \approx c_s k$, where c_s is the adiabatic speed of sound, $c_s = c_T \sqrt{1+2/d_f}$ for an ideal gas. For the velocity components, the transverse components $S_{k,\omega}^{(v_\perp)}$ exhibit all three peaks, while the longitudinal component $S_{k,\omega}^{(v_\parallel)}$ lacks the central peak, as seen in the figure. Note that as the fluid becomes less compressible (i.e., the speed of sound increases), there is an increasing separation of time-scales between the side and central spectral peaks, showing the familiar numerical stiffness of the full compressible Navier–Stokes equations.

We have verified that for small wavevectors the numerical dynamic structure factors are in excellent agreement with the analytical predictions, even for such large time steps. For wavevectors that are not small compared to the discretization limits we do not expect a perfect dynamic structure factor, even for very small

time steps. It is important, however, that the discretization behave reasonably for all wavevectors (e.g., there should be no spurious maxima), and be somewhat accurate for intermediate wavevectors, even for large time steps. As seen in Figure 4, the RK3D-2RNG algorithm seems to perform well even with a large time step. Improving the accuracy at larger wavevectors requires using higher-order spatial differencing [50] (see discussion in Section 5C), compact stencils (linear solvers) [48], or pseudospectral methods [30], each of which has certain advantages but also significant disadvantages over the finite-volume approach in a more general nonlinear nonequilibrium context.

8. Summary and concluding remarks

We analyzed finite-volume schemes for the linearized Landau–Lifshitz Navier–Stokes (LLNS) system (4) and related SPDEs such as the stochastic advection-diffusion Equation (35). Our approach to studying the accuracy of these explicit schemes is based on evaluating the discrete static and dynamic structure factors, focusing on the accuracy at small wavenumber $\Delta k = k\Delta x$ and wavefrequency $\Delta\omega = \omega\Delta t$. The methodology for formulating the structure factor for numerical schemes is developed in Section 3, and then specialized to stochastic conservation laws in Section 4. Applying this analysis to the stochastic heat Equation (42) in Section 5 we find the truncation error for the Euler method to be $O(\Delta t k^2)$; the error for a standard predictor-corrector scheme is $O(\Delta t^2 k^4)$ using the same random numbers in the predictor and corrector stages but $O(\Delta t^3 k^6)$ using independent random numbers at each stage. Section 6 extends this analysis to the third-order Runge–Kutta scheme of Bell et al. [13; 10] for the one-dimensional advection-diffusion SPDE. We find the best accuracy when the stochastic fluxes at the three stages are generated from two sets of random numbers, as given by (62); using this version, called RK3-2RNG, for the LLNS equations gives good results, even when nonlinear effects are included (see Figures 2–4). Finally, Section 7 explains why the cross-correlations in the stress tensor in the three-dimensional LLNS require special treatment and proposes a mixed MAC/Fortin discretization as a way to obtain the desired discrete fluctuation-dissipation balance.

Here we have investigated linearized PDEs with stochastic fluxes where the noise is additive. As such, the stability properties of the numerical schemes are the same as for the deterministic case. Yet in practice one would like to implement these schemes for the nonlinear stochastic PDEs with state-dependent stochastic fluxes. While in the limit of small fluctuations the behavior of the schemes is expected to be similar to the linearized case, the proper mathematical foundation and even formulation of the nonlinear fluctuating equations has yet to be laid out. Furthermore, the stability properties of numerical schemes for the nonlinear

LLNS system are not well understood and the whole notion of stability is different than it is for deterministic schemes. For example, even at equilibrium, a rare fluctuation can cause a thermodynamic instability (e.g., a negative temperature which implies a complex sound speed) or a mechanical instability (e.g., a negative mass density). Capping the noises in the stochastic flux terms will not necessarily solve the problem because the hydrodynamic variables are time-correlated so the numerical instability may not appear on a single step but rather as an accumulated effect. We are investigating these issues and will discuss strategies to address this type of stability issue in future publications.

One of the advantages of finite volume solvers over spectral methods is the ability to implement realistic, complex geometries for fluid simulations. In this paper we only consider periodic boundaries but many other boundary conditions are of interest, notably, impenetrable flat hard walls with stick and slip conditions for the velocities and either adiabatic (zero temperature gradient) or thermal (constant temperature) conditions for the temperature. Equilibrium statistical mechanics requires that the static structure factor be oblivious to the presence of walls, even though the dynamic structure factors typically exhibit additional peaks due to the reflections of fluctuations from the boundaries [25]. Therefore, the numerical discretization of the Laplacian operator L, the divergence operator D and the covariance of the stochastic fluxes C should continue to satisfy the discrete fluctuation-dissipation balance condition $L + L^\star = -2DCD^\star$ and be consistent, even in the presence of boundaries. Standard treatments of boundary conditions used in deterministic schemes can easily be implemented in the stochastic setting [13; 6], however, satisfying the discrete fluctuation-dissipation balance is not trivial and requires modifying the stochastic fluxes and possibly also the finite-difference stencils near the boundaries [6], as briefly discussed in the Appendix to [25]. In particular, the case of Dirichlet boundary conditions is more complicated, especially in the case of the mixed MAC and Fortin discretization of the compressible Navier–Stokes equations. Complex boundaries present further challenges even in the deterministic setting. We will explore the issues associated will fluctuations at physical boundaries in future publications.

One motivation for the development of numerical methods for the LLNS equations is for their use in multialgorithm hybrids. One emerging paradigm in the modeling and simulation of multiscale problems is multialgorithm refinement (MAR). MAR is a general simulation approach that combines two or more algorithms, each of which is appropriate for a different scale regime. MAR schemes typically couple structurally different computational schemes such as particle-based molecular simulations with continuum partial differential equation (PDE) solvers. The general idea is to perform detailed calculations using an accurate but expensive algorithm in a small region (or for a short time), and couple this computation to

a simpler, less expensive method applied to the rest. The major difficulty is in constructing hybrid is that particle and continuum methods treat thermal noise (fluctuations) in completely different ways. The challenge is to ensure that the numerical coupling of the particle and continuum computations is self-consistent, stable, and most importantly, does not adversely impact the underlying physics. These problems become particularly acute when one wants to accurately capture the physical fluctuations at micro- and mesoscopic scales. The correct treatment of boundary conditions in stochastic PDE schemes is particularly difficult yet crucial in hybrid schemes since the coupling of the two algorithms is essentially a dynamic, two-way boundary condition. Recent work by Tysanner et al. [62], Foo et al. [12], Williams et al. [64] and Donev et al. [25] has demonstrated the need to model fluctuations at the continuum level in hybrid continuum / particle approaches, however, a seamless coupling has yet to be developed.

In this paper we consider the fully compressible LLNS system, for many of the phenomena of interest the fluid flow aspects occur at very low Mach numbers. Another topic of future work for stochastic PDE schemes is to construct a low Mach number fluctuating hydrodynamics algorithm. A number of researchers have considered extended versions of the incompressible Navier–Stokes equations that include a stochastic stress tensor [56; 61; 8]. This type of model does introduce fluctuations into the Navier–Stokes equations and is applicable in some settings, such as in modeling simple Brownian motion. However, as pointed out by Zaitsev and Shliomis [66], the incompressible approximation introduces fictitious correlations between the velocity components of the fluid. Furthermore, this type of approach does not capture the full range of fluctuations in the compressible equations. In particular, adding a stochastic stress into the incompressible Navier–Stokes equations creates fluctuations in velocity but does not reproduce the large scale and slow fluctuations in density and temperature, which persist even in the incompressible limit. We plan to investigate alternative formulations that can capture more of the features of the fluctuating hydrodynamics while still exploiting the separation of scales inherent in low Mach number flows. We also note that although the theoretical importance of distinguishing between the incompressible approximation and the low Mach number limit is well established for fluctuating hydrodynamics [14; 67], numerical algorithms for the latter have yet to be developed.

Appendix: Semi-implicit Crank–Nicolson method

When sound is included in the fluctuating hydrodynamic equations implicit methods are not really beneficial since the large sound speed limits the time step. However, for the pure stochastic diffusion/heat equation or advection-diffusion equations with a small advection speed the time step may become strongly limited by the

diffusive CFL limit, especially for small cells. In such cases an implicit method can be used to lift the diffusive stability restriction on the time step. For example, the second-order (in both space and time) Crank–Nicolson semi-implicit scheme for the stochastic heat equation entails solving the linear system

$$u_j^{n+1} - \frac{\mu \Delta t}{2 \Delta x^2}(u_{j-1}^{n+1} - 2u_j^{n+1} + u_{j+1}^{n+1})$$

$$= u_j^n + \frac{\mu \Delta t}{2 \Delta x^2}(u_{j-1}^n - 2u_j^n + u_{j+1}^n) + \sqrt{2\mu}\,\frac{\Delta t^{1/2}}{\Delta x^{3/2}}(W_{j+1/2}^n - W_{j-1/2}^n), \quad \text{(A.1)}$$

which is tridiagonal except at periodic boundaries.

The analysis carried out above for explicit schemes can easily be extended to implicit methods since in Fourier space different wavevectors again decouple and the above iteration becomes a scalar linear equation for $\hat{u}_k^{n+1}$ that can trivially be solved. Firstly, it is observed that the small time step limit is the same regardless of the semi-implicit treatment, specifically, the same discrete fluctuation-dissipation condition (31) applies. Remarkably, for the Crank–Nicolson iteration (A.1) it is found that the discrete static structure factor is independent of the time step, $S_k = 1$ for all β. The dynamic structure factor, however, has the same spatial discretization errors (48) as for the Euler scheme even in the limit $\beta \rightarrow 0$. Furthermore, as expected, the dynamics is not accurate for large β and the time step cannot be enlarged much beyond the diffusive stability limit related to the smallest length-scale at which one wishes to correctly resolve the dynamics of the fluctuations.

If advection is included as well and also discretized semi-implicitly, the method again gives perfect structure factors, $S_k = 1$ identically, and is unconditionally stable. If only diffusion is handled semi-implicitly but advection is handled with a predictor-corrector approach, then it turns out that the optimal method is to not include a stochastic flux in the predictor step, giving the same leading-order error term as PC-2RNG in (55) when $|r| > 0$, but giving a perfect $S_k = 1$ when $r = 0$.

Acknowledgments

References

[1] R. Adhikari, K. Stratford, M. E. Cates, and A. J. Wagner, *Fluctuating lattice boltzmann*, Europhysics Letters **71** (2005), 473–479.

[2] F. J. Alexander and A. L. Garcia, *The direct simulation Monte Carlo method*, Computers in Physics **11** (1997), no. 6, 588–593.

[3]   A. S. Almgren, J. B. Bell, and W. G. Szymczak, *A numerical method for the incompressible Navier–Stokes equations based on an approximate projection*, SIAM J. Sci. Comput. **17** (1996), no. 2, 358–369. MR 96j:76104 Zbl 0845.76055

[4]   R. D. Astumian and P. Hanggi, *Brownian motors*, Physics Today (2002), 33–39.

[5]   P. J. Atzberger, *Stochastic eulerian-lagrangian methods for fluid-structure interactions with thermal fluctuations and shear boundary conditions*, Preprint. arXiv 0910.5739

[6]   _____ , *Spatially adaptive stochastic numerical methods for intrinsic fluctuations in reaction-diffusion systems*, Journal of Computational Physics **229** (2010), no. 9, 3474 – 3501.

[7]   P. J. Atzberger, P. R. Kramer, and C. S. Peskin, *A stochastic immersed boundary method for fluid-structure dynamics at microscopic length scales*, J. Comput. Phys. **224** (2007), no. 2, 1255–1292. MR 2008g:74031 Zbl 1124.74052

[8]   _____ , *A stochastic immersed boundary method for fluid-structure dynamics at microscopic length scales*, J. Comput. Phys. **224** (2007), no. 2, 1255–1292. MR 2008g:74031 Zbl 1124.74052

[9]   W. Bao and S. Jin, *High-order I-stable centered difference schemes for viscous compressible flows*, J. Comput. Math. **21** (2003), no. 1, 101–112. MR 2004c:65084 Zbl 1086.76052

[10] J. B. Bell, A. Garcia, and S. Williams, *Computational fluctuating fluid dynamics*, ESAIM: Mathematical Modelling and Numerical Analysis (2010), To appear.

[11] J. B. Bell, P. Colella, and H. M. Glaz, *A second-order projection method for the incompressible Navier–Stokes equations*, J. Comput. Phys. **85** (1989), no. 2, 257–283. MR 90i:76002 Zbl 0681.76030

[12] J. B. Bell, J. Foo, and A. L. Garcia, *Algorithm refinement for the stochastic Burgers' equation*, J. Comput. Phys. **223** (2007), no. 1, 451–468. MR 2008a:65010

[13] J. B. Bell, A. L. Garcia, and S. A. Williams, *Numerical methods for the stochastic Landau–Lifshitz Navier–Stokes equations*, Phys. Rev. E (3) **76** (2007), no. 1, 016708, 12. MR 2008i:76137

[14] I. Bena, F. Baras, and M. M. Mansour, *Hydrodynamic fluctuations in the Kolmogorov flow: Nonlinear regime*, Phys. Rev. E **62** (2000), no. 5, 6560–6570.

[15] I. Bena, M. Malek Mansour, and F. Baras, *Hydrodynamic fluctuations in the Kolmogorov flow: linear regime*, Phys. Rev. E (3) **59** (1999), no. 5, part B, 5503–5510. MR 1690930

[16] J. Borrill and M. Gleiser, *Matching numerical simulations to continuum field theories: A lattice renormalization study*, Nuclear Phys. B **483** (1997), 416–428.

[17] A. J. Chorin, *Numerical solution of the Navier–Stokes equations*, Math. Comp. **22** (1968), 745–762. MR 39 #3723 Zbl 0198.50103

[18] P. Collela and P. R. Woodward, *The piecewise parabolic method (ppm) for gas dynamics calculations*, J. Comp. Phys **54** (1984), 174.

[19] G. Da Prato, *Kolmogorov equations for stochastic PDEs*, Birkhäuser, Basel, 2004. MR : MR 2005m:60002 Zbl 1066.60061

[20] J. M. O. de Zarate and J. V. Sengers, *Hydrodynamic fluctuations in fluids and fluid mixtures*, Elsevier Science, 2007.

[21] A. Debussche and J. Printems, *Weak order for the discretization of the stochastic heat equation*, Math. Comp. **78** (2009), no. 266, 845–863. MR 2010f:60192

[22] R. Delgado-Buscalioni and A. Dejoan, *Nonreflecting boundaries for ultrasound in fluctuating hydrodynamics of open systems*, Phys. Rev. E **78** (2008), no. 4, 046708.

[23] R. Delgado-Buscalioni and G. D. Fabritiis, *Embedding molecular dynamics within fluctuating hydrodynamics in multiscale simulations of liquids*, Phys. Rev. E **76** (2007), no. 3, 036709.

[24] C. V. den Broeck, R. Kawai, and P. Meurs, *Exorcising a Maxwell demon*, Phys. Rev. Lett. **93** (2004), 090601.

[25] A. Donev, J. B. Bell, A. L. Garcia, and B. J. Alder, *A hybrid particle-continuum method for hydrodynamics of complex fluids*, SIAM J. Multiscale Modeling and Simulation **8** (2010), no. 3, 871–911.

[26] B. Dünweg, U. D. Schiller, and A. J. C. Ladd, *Statistical mechanics of the fluctuating lattice Boltzmann equation*, Phys. Rev. E (3) **76** (2007), no. 3, 036704, 10. MR 2008i:82096

[27] J. Eggers, *Dynamics of liquid nanojets*, Phys. Rev. Lett. **89** (2002), no. 8, 084502.

[28] P. Español, *Stochastic differential equations for non-linear hydrodynamics*, Physica A **248** (1998), no. 1-2, 77–96.

[29] G. D. Fabritiis, M. Serrano, R. Delgado-Buscalioni, and P. V. Coveney, *Fluctuating hydrodynamic modeling of fluids at the nanoscale*, Phys. Rev. E **75** (2007), no. 2, 026307.

[30] B. Fornberg, *A practical guide to pseudospectral methods*, Cambridge Monographs on Applied and Computational Mathematics, no. 1, Cambridge University Press, Cambridge, 1996. MR 97g:65001 Zbl 0844.65084

[31] M. Fortin, *Numerical solution of the steady state Navier–Stokes equations*, Numerical Methods in Fluid Dynamics (J. J. Smolderen, ed.), Technical Editing and Reproduction Ltd., London, 1972, pp. 5.1–5.7 AGARD–LS–48.

[32] A. L. Garcia, M. M. Mansour, G. Lie, and E. Clementi, *Numerical integration of the fluctuating hydrodynamic equations*, J. Stat. Phys. **47** (1987), 209.

[33] A. L. Garcia and C. Penland, *Fluctuating hydrodynamics and principal oscillation pattern analysis*, J. Stat. Phys. **64** (1991), 1121.

[34] C. W. Gardiner, *Handbook of stochastic methods for physics, chemistry and the natural sciences*, 3rd ed., Springer Series in Synergetics, no. 13, Springer, Berlin, 2004. MR 2004m:00008 Zbl 1143.60001

[35] G. Giupponi, G. D. Fabritiis, and P. V. Coveney, *Hybrid method coupling fluctuating hydrodynamics and molecular dynamics for the simulation of macromolecules*, J. Chem. Phys. **126** (2007), no. 15, 154903.

[36] J. Goodman and A. D. Sokal, *Multigrid Monte Carlo method: Conceptual foundations*, Phys. Rev. D **40** (1989), no. 6, 2035–2071.

[37] S. Gottlieb and C.-W. Shu, *Total variation diminishing Runge–Kutta schemes*, Math. Comp. **67** (1998), no. 221, 73–85. MR 98c:65122 Zbl 0897.65058

[38] F. H. Harlow and J. E. Welch, *Numerical calculation of time-dependent viscous incompressible flow of fluids with free surfaces*, Physics of Fluids **8** (1965), 2182–2189.

[39] A. Jentzen and P. E. Kloeden, *The numerical approximation of stochastic partial differential equations*, Milan J. Math. **77** (2009), 205–244. MR 2578878 Zbl 1186.65011

[40] K. Kadau, C. Rosenblatt, J. L. Barber, T. C. Germann, Z. Huang, P. Carles, and B. J. Alder, *The importance of fluctuations in fluid mixing*, PNAS **104** (2007), no. 19, 7741–7745.

[41] K. Kadau, T. C. Germann, N. G. Hadjiconstantinou, P. S. Lomdahl, G. Dimonte, B. L. Holian, and B. J. Alder, *Nanohydrodynamics simulations: an atomistic view of the Rayleigh–Taylor instability*, Proc. Natl. Acad. Sci. USA **101** (2004), no. 16, 5851–5855. MR 2004m:76077 Zbl 1063.76029

[42] W. Kang and U. Landman, *Universality crossover of the pinch-off shape profiles of collapsing liquid nanobridges in vacuum and gaseous environments*, Phys. Rev. Lett. **98** (2007), no. 6, 064504.

[43] P. R. Kramer, C. S. Peskin, and P. J. Atzberger, *On the foundations of the stochastic immersed boundary method*, Comput. Methods Appl. Mech. Engrg. **197** (2008), no. 25-28, 2232–2249. MR 2009d:60269 Zbl 1158.76420

[44] R. Kubo, *The fluctuation-dissipation theorem*, Reports on Progress in Physics **29** (1966), no. 1, 255–284.

[45] A. J. C. Ladd, *Short-time motion of colloidal particles: Numerical simulation via a fluctuating lattice-Boltzmann equation*, Phys. Rev. Lett. **70** (1993), no. 9, 1339–1342.

[46] L. D. Landau and E. M. Lifshitz, *Fluid mechanics*, Course of Theoretical Physics, no. 6, Pergamon Press, London, 1959. MR 21 #6839 Zbl 0146.22405

[47] J. L. Lebowitz, E. Presutti, and H. Spohn, *Microscopic models of hydrodynamic behavior*, J. Statist. Phys. **51** (1988), no. 5-6, 841–862. MR 90c:60072 Zbl 1086.60531

[48] S. K. Lele, *Compact finite difference schemes with spectral-like resolution*, J. Comput. Phys. **103** (1992), no. 1, 16–42. MR 93g:76086 Zbl 0759.65006

[49] A. Lemarchand and B. Nowakowski., *Fluctuation-induced and nonequilibrium-induced bifurcations in a thermochemical system*, Molecular Simulation **30** (2004), no. 11-12, 773–780.

[50] K. Mahesh, *A family of high order finite difference schemes with good spectral resolution*, J. Comput. Phys. **145** (1998), no. 1, 332–358. MR 99d:76068 Zbl 0926.76081

[51] M. M. Mansour, A. L. Garcia, G. C. Lie, and E. Clementi, *Fluctuating hydrodynamics in a dilute gas*, Phys. Rev. Lett. **58** (1987), 874–877.

[52] M. M. Mansour, C. V. den Broeck, I. Bena, and F. Baras, *Spurious diffusion in particle simulations of the Kolmogorov flow*, Europhysics Letters **47** (1999), no. 1, 8–13.

[53] M. Mareschal, M. M. Mansour, G. Sonnino, and E. Kestemont, *Dynamic structure factor in a nonequilibrium fluid: A molecular-dynamics approach*, Phys. Rev. A **45** (1992), 7180–7183.

[54] P. Meurs, C. V. den Broeck, and A. L. Garcia, *Rectification of thermal fluctuations in ideal gases*, Phys. Rev. Lett. E **70** (2004), 051109.

[55] E. Moro, *Hybrid method for simulating front propagation in reaction-diffusion systems*, Phys. Rev. E **69** (2004), no. 6, 060101.

[56] M. Moseler and U. Landman, *Formation, stability, and breakup of nanojets*, Science **289** (2000), no. 5482, 1165–1169.

[57] B. Nowakowski and A. Lemarchand, *Sensitivity of explosion to departure from partial equilibrium*, Phys. Rev. E **68** (2003), 031105.

[58] G. Oster, *Darwin's motors*, Nature **417** (2002), 25.

[59] Y. Pomeau and P. Résibois, *Time dependent correlation functions and mode-mode coupling theories*, Phys. Rep. **19** (1975), 63–139.

[60] G. Quentin and I. Rehberg, *Direct measurement of hydrodynamic fluctuations in a binary mixture*, Phys. Rev. Lett. **74** (1995), no. 9, 1578–1581.

[61] N. Sharma and N. A. Patankar, *Direct numerical simulation of the Brownian motion of particles by using fluctuating hydrodynamic equations*, J. Comput. Phys. **201** (2004), 466–486.

[62] M. Tysanner and A. L. Garcia, *Non-equilibrium behavior of equilibrium reservoirs in molecular simulations*, Int. J. Numer. Meth. Fluids **48** (2005), 1337–1349.

[63] N. K. Voulgarakis and J.-W. Chu, *Bridging fluctuating hydrodynamics and molecular dynamics simulations of fluids*, J. Chem. Phys. **130** (2009), no. 13, 134111.

[64] S. A. Williams, J. B. Bell, and A. L. Garcia, *Algorithm refinement for fluctuating hydrodynamics*, Multiscale Model. Simul. **6** (2007), no. 4, 1256–1280. MR 2009c:76059 Zbl 05381404

[65] M. Wu, G. Ahlers, and D. S. Cannell, *Thermally induced fluctuations below the onset of Rayleigh–Bénard convection*, Phys. Rev. Lett. **75** (1995), no. 9, 1743–1746.

[66] V. M. Zaitsev and M. I. Shliomis, *Hydrodynamic fluctuations near convection threshold*, Sov. Phys. JETP **32** (1971), 866.

[67] R. Zwanzig and M. Bixon, *Compressibility effects in the hydrodynamic theory of Brownian motion*, Journal of Fluid Mechanics **69** (1975), 21–25.

ALEKSANDAR DONEV: aleks.donev@gmail.com
Lawrence Berkeley National Laboratory, Center for Computational Sciences and Engineering, MS 50A-1148, LBL, 1 Cyclotron Rd., Berkeley 94720, United States
http://cims.nyu.edu/~donev

ERIC VANDEN-EIJNDEN: eve2@cims.nyu.edu
New York University, Courant Institute of Mathematical Sciences, New York 10012, United States

ALEJANDRO GARCIA: algarcia@algarcia.org
San Jose State University, Department of Physics and Astronomy, San Jose, CA 95192, United States

JOHN BELL: jbbell@lbl.gov
Lawrence Berkeley National Laboratory, Center for Computational Science and Engineering, Berkeley, CA 94720, United States

Communications in Applied Mathematics and Computational Science

pjm.math.berkeley.edu/camcos

See inside back cover or pjm.math.berkeley.edu/camcos for submission instructions.

Communications in Applied Mathematics and Computational Science